NMR Studies of Hindered Ligand Rotation, Magnetic Anisotropy, Curie Behavior, Proton Spin Relaxation, and Ligand Exchange in Some Novel Oxomolybdenum(V)/Iron(III) Porphyrinate Complexes

Partha Basu, Nikolai V. Shokhirev, John H. Enemark,* and F. Ann Walker*

Contribution from the Department of Chemistry, University of Arizona, Tucson, Arizona 85721

Received March 30, 1995[⊗]

Abstract: A detailed ^{1}H NMR study has been carried out on the novel porphyrinatoiron(III)−Mo(V) complexes {tri-*p*-tolyl[2,3-[((hydrotris(3,5-dimethylpyrazolyl)borato)oxomolybdenum)dioxy]phenyl]porphyrinato}bis(L)iron-(III) chloride, $[Fe(2,3\text{-Mo-TTP})L_2]^+Cl^-$, where L = *N*-methylimidazole (NMeIm), imidazole (ImH), or 4-(dimethylamino)pyridine (4DAP), and $[Fe(3,4\text{-Mo-TTP})(NMeIm)_2]^+Cl^-$. Each of these compounds contains two $S = 1/2$ metal centers. In the 2,3-isomer, rotation of one of the axial ligands bound to the iron atom is prevented by the bulky (hydrotris(pyrazolyl)borato)oxomolybdenum substituent, as evidenced by the observation of eight unique pyrrole-H resonances that do not coalesce over most of the liquid range of the CD_2Cl_2 solvent (−90 to +30 °C). Moreover, the slow electron spin relaxation time of oxomolybdenum(V) allows this center to function as a "dipolar relaxation agent" that provides a sensitive measure of the distance between the Mo(V) center and each of the pyrrole protons of the low-spin iron(III) porphyrinate. Combination of results from measurement of the T_1s of the eight pyrrole protons, the COSY coupling pattern, NOEs between protons not in the same pyrrole ring, and analysis of the effect of the orientation of the nodal plane of the nonrotating axial ligand on the rhombic dipolar contribution to the isotropic shift led to a complete and unambiguous assignment of these resonances. Theoretical analysis of the observed shifts and their temperature dependence made it possible to map the unpaired electron spin density at the β-pyrrole positions, and thereby the unpaired electron spin density distribution in the π orbital into which the unpaired electron is preferentially delocalized, and to calculate the approximate energy separation, ΔE_π, between it and its e(π) counterpart. Thermal population of the higher-energy orbital accounts for the non-zero intercepts of the Curie plots of the pyrrole-H resonances. Comparison to other systems, including the 3,4-MoO complex, demonstrates the large, dominating effect of a fixed axial ligand plane in determining the spread of the pyrrole-H resonances. The results demonstrate the relatively small effect of the orientation of the p_π orbital of the planar ligand on the in-plane magnetic anisotropy, and its much larger effect on spin delocalization *via* the contact interaction. Thus, we conclude that it is likely that the spread of the methyl resonances in ferricytochromes b_5 and *c* and other low-spin ferriheme proteins is controlled largely by the effect of the orientation of the p_π orbital of the strongest π donor ligand on the *contact* shift, rather than on the in-plane magnetic anisotropy created simultaneously by that same p_π orbital and manifested in the dipolar term. Rates of axial ligand (L) exchange for $[Fe(2,3\text{-Mo-TTP})L_2]^+Cl^-$ (for L = NMeIm and 4DAP) have also been measured. It is found that the ligand on the same side of the porphyrinate plane (*syn*) as the bulky oxomolybdenum(V) group exchanges much more slowly than the one on the opposite side of the porphyrinate plane (*anti*).

Introduction

For some time we have been interested in two factors that may affect the size of the contact shifts of low-spin iron(III) model hemes and heme proteins: (1) heme substituents[1] and (2) axial ligand plane orientation.[1-4] Both of these factors have previously been shown to be important in determining the proton NMR shifts of heme proteins,[5-9] as well as other spectroscopic and redox properties. However, in studies of the heme proteins it has been difficult to quantify the contribution of each of these effects to the observed spectroscopic and redox properties. Moreover, other factors such as the hydrophobicity of the heme binding pocket, off-axis tilting of axial histidines, hydrogen-bonding of the histidine N−H to protein residues, and surface charge of the protein may also be important. We have undertaken investigations of model hemes designed to test

[⊗] Abstract published in *Advance ACS Abstracts*, August 15, 1995.

(1) Walker, F. A.; Simonis, U. Proton NMR Spectroscopy of Model Hemes. In *Biological Magnetic Resonance, Vol. 12: NMR of Paramagnetic Molecules*; Berliner, L. J., Reuben, J., Eds.; Plenum Press: New York; 1993; pp 133−274 and references therein.

(2) Walker, F. A.; Huynh, B. H.; Scheidt, W. R.; Osvath, S. R. *J. Am. Chem. Soc.* **1986**, *108*, 5288−5297.

(3) Walker, F. A.; Simonis, U.; Zhang, H.; Walker, J. M.; Ruscitti, T. M.; Kipp, C.; Amputch, M. A.; Castillo, B. V.; Cody, S. H.; Wilson, D. L.; Graul, R. E.; Yong, G. J.; Tobin, K.; West, J. T.; Barichievich, B. A. *New J. Chem.* **1992**, *16*, 609−620.

(4) . (a) Walker, F. A., presented at the NATO Advanced Study Workshop on NMR Spectroscopy of Paramagnetic Metalloproteins, Sintra, Portugal, June 1994. (b) Shokhirev, N. V.; Walker, F. A. Submitted for publication.

(5) (a) Satterlee, J. D. *Annu. Rep. NMR Spectrosc.* **1986**, *17*, 79. (b) Satterlee, J. D. In *Metal Ions in Biological Systems*; Sigel, H., Ed.; Marcel Dekker: New York, 1986; Vol. 21, p 121.

(6) La Mar, G. N.; de Ropp, J. S. NMR Methodology for Paramagnetic Proteins. In *Biological Magnetic Resonance, Vol 12: NMR of Paramagnetic Molecules*; Berlinger, L. J., Reuben, J., Eds.; Plenum Press: New York, 1993; pp 1−111.

(7) (a) Turner, D. L. *Eur. J. Biochem.* **1993**, *211*, 563. (b) Santos, H.; Turner, D. L. *Magn. Reson. Chem.* **1993**, *31*, S90. (c) Santos, H.; Turner, D. L. *Biochim. Biophys. Acta* **1988**, *954*, 277−286.

(8) Bertini, I.; Luchinat, C. In *NMR of Paramagnetic Molecules in Biological Systems*; Bowen, D. L., Hubit, G., Myson-Etherington, D., Eds.; Benjamin-Cummings: Menlo Park, CA, 1986.

(9) Wu, J.-Z.; La Mar, G. N.; Yu, L. P.; Lee, K.-B.; Walker, F. A.; Chiu, M.; Sliger, S. G. *Biochemistry* **1991**, *30*, 2156−2165.

0002-7863/95/1517-9042$09.00/0

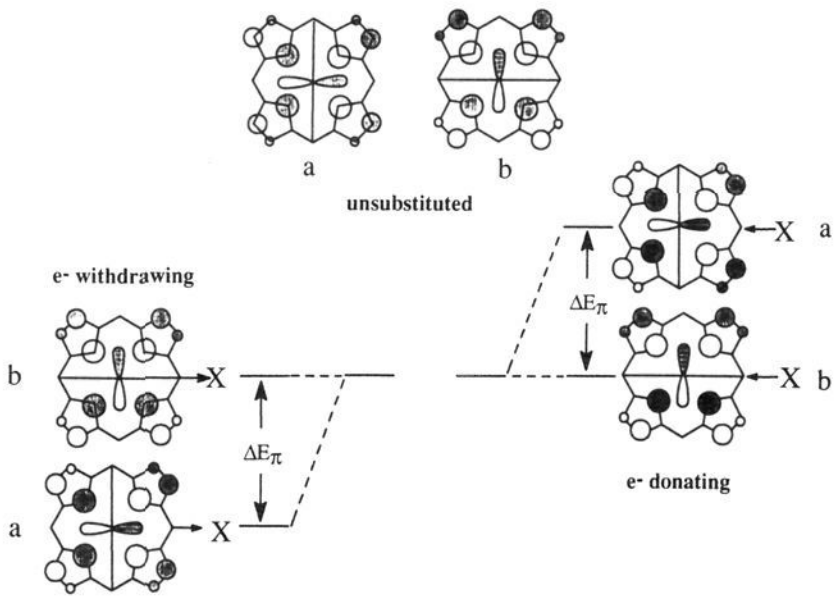

Figure 1. Formation of molecular orbitals by the interaction of the porphyrin 3e(π) orbitals[11] and the d_π metal orbitals produces a low-energy e(π) bonding MO set that is mainly porphyrin in character and is completely filled and a higher energy (valence) "antibonding" MO set that is mainly metal in character and contains three electrons. Only the higher energy "antibonding" valence set is shown in the center of the figure. Placing a unique substituent at one of the *meso* positions lifts the degeneracy and gives rise to up to four different electron densities at the pyrrole positions. The relative energies of the two valence e(π) orbitals if the unique *meso* substituent is electron withdrawing are shown on the left side of the figure, and those for the case of the unique *meso* substituent being electron donating are shown on the right side. The unpaired electron is thus preferentially placed in the highest-energy orbital. If at least one planar axial ligand is prevented from rotating and its nodal plane is slightly misaligned with that of the unique *meso* substituent, then all eight pyrrole carbons will have uniquely different unpaired electron spin densities (see Results and Discussion).

separately the importance of heme substituents[1] and axial ligand plane orientation.[2-4] As the present work will clearly show, both of these factors have major effects upon the energies of and electron distributions in the valence e(π) orbitals of the heme.[1,10] For low-spin Fe(III), the 3e(π) orbitals of the porphyrin ring[11,12] and the d_π orbitals of the metal can overlap to form two filled low-energy molecular orbitals that are mainly porphyrin in character and two high-energy (valence) molecular orbitals that are mainly metal in character and contain three electrons.[10] The odd electron in the higher-energy set, which is shown schematically in Figure 1, gives rise to the spin delocalization that results in the observed contact shift pattern.[1,10]

We have recently shown[10] that a single *meso*-carbon heme substituent that is strongly electron-donating or -withdrawing relative to the others can cause significant redistribution of spin density around the porphyrin ring, due to the readjustment of orbital coefficients within the valence e(π) MOs. Such substituent effects typically cause splitting, ΔE_π, of the formerly degenerate valence e(π) orbitals by only tens of cm^{-1},[1,10] as shown in Figure 1, and thus both orbitals are utilized for spin delocalization to a significant extent as the temperature is varied, according to their nearly-equal but varying Boltzmann populations. As we will show below, a planar axial ligand that is prevented from rotation by specially-designed model compounds or by hydrogen-bonding of a histidine or crowding of a methionine ligand within the heme pocket of a heme protein can enforce a much larger energy difference ΔE_π between the two valence e(π) molecular orbitals of the heme.[4] Since the electron that is added upon reduction of Fe(III) to Fe(II) will go into the higher energy of these two valence e(π) molecular orbitals, the reduction potentials of model hemes and heme proteins may be modulated by the relative energies of the two valence e(π) molecular orbitals.[2] This difference in energy is clearly evidenced in the EPR spectra recorded at low temperatures.[2] These relative energies are determined by a combination of the value of ΔE_π and the energy that measures the ligand field strength of the axial ligands. The design of model hemes that can be utilized to test the importance of axial ligand plane orientation on the pattern of unpaired electron spin delocalization in the porphyrin ring has long been frustrated by the extremely low barriers to rotation of axial ligands about the Fe–L bonds[13,14] and the ease of deformation of the porphyrinate core when large *ortho* substituents are placed on the phenyl rings of tetraphenylporphyrin (TPP).[15-17] Covalent attachment of the axial ligands to the porphyrinate ring might seem to be the most straightforward means of ensuring a fixed axial ligand orientation, and this method has been investigated,[18-21] with limited success. The problems that arise result mainly from (1) the presence of multiple conformations of the covalently attached ligand arm that lead to multiple orientations of the axial ligand,[22] which in turn give rise to many more than the desired number of resonances,[20,21] and (2) the loss of stability of the Fe–L bond due to the loss of entropy of internal rotation around the single bonds of the uncoordinated form of the ligand upon binding to the metal.[23,24] Thus, attempts have been made to create specific axial ligand orientations by steric crowding.[3,18,25] However, in all of these cases, the axial ligands were able to rotate, at least at room temperature,[3] and hence, the large spread of the eight pyrrole proton resonances observed at low temperatures decreases and goes through a chemical exchange collapse to four lines as the temperature is increased. We were therefore extremely pleased to find that the novel porphyrinatoiron(III)–Mo(V) complexes, {tri-*p*-tolyl[2,3-[((hydrotris(3,5-dimethylpyrazolyl)borato)oxomolybdenum)dioxy]phenyl]porphyrinato}-bis(L)iron(III) chloride [Fe(2,3-Mo-TTP)L_2]Cl, where L is a Lewis base, whose synthesis,[26,27] electrochemistry, and EPR

(10) Tan, H.; Simonis, U.; Shokhirev, N. V.; Walker, F. A. *J. Am. Chem. Soc.* **1994**, *116*, 5784–5790.

(11) Longuet-Higgins, H. C.; Rector, C. W.; Platt, R. R. *J. Chem. Phys.* **1950**, *18*, 1174–1181.

(12) (a) Streitwieser, A., Jr. *Molecular Orbital Theory for Organic Chemists*; John Wiley: New York, 1961. (b) Greenwood, H. H. *Computing Methods in Quantum Organic Chemistry;* Wiley-Interscience: New York, 1972.

(13) Safo, M. K.; Walker, F. A.; Raitsimring, A. M.; Walters, W. P.; Dolata, D. P.; Debrunner, P. G.; Scheidt, W. R. *J. Am. Chem. Soc.* **1994**, *116*, 7760–7770.

(14) (a) Nakamura, M.; Groves, J. T. *Tetrahedron* **1988**, *44*, 3225–3230. (b) Nakamura, M.; Nakamura, N. *Chem. Lett.* **1991**, 627–630. (c) Nakamura, M.; Tajima, K.; Tada, K.; Ishizu, K.; Nakamura, N. *Inorg. Chim. Acta* **1994**, *224*, 113–124.

(15) Safo, M. K.; Gupta, G. P.; Walker, F. A.; Scheidt, W. R. *J. Am. Chem. Soc.* **1991**, *43*, 5497–5510.

(16) Safo, M. K.; Gupta, G. P.; Watson, C. T.; Simonis, U.; Walker, F. A.; Scheidt, W. R. *J. Am. Chem. Soc.* **1992**, *114*, 7066–7075.

(17) Munro, O. Q.; Marques, H. M.; Debrunner, P. G.; Mohanrao, K.; Scheidt, W. R. *J. Am. Chem. Soc.* **1995**, *117*, 935–954.

(18) Walker, F. A. *J. Am. Chem. Soc.* **1980**, *102*, 3254–3256.

(19) Goff, H. M. *J. Am. Chem. Soc.* **1980**, *102*, 3252–3254.

(20) Traylor, T. G.; Berzinis, A. P. *J. Am. Chem. Soc.* **1980**, *102*, 2844–2846.

(21) Walker, F. A.; Reis, D.; Balke, V. L. *J. Am. Chem. Soc.* **1984**, *106*, 6888–6898.

(22) Bobrik, M. A.; Walker, F. A. *Inorg. Chem.* **1980**, *19*, 3383–3390.

(23) Walker, F. A.; Benson, M. *J. Am. Chem. Soc.* **1980**, *102*, 5530–5538.

(24) Lopez, M. A.; Ybarra, C. D.; Hyatt, S. *Inorg. Chim. Acta* **1995**, *231*, 121-131.

(25) Walker, F. A.; Buehler, J.; West, J. T.; Hinds, J. L. *J. Am. Chem. Soc.* **1983**, *105*, 6923–6929.

(26) LaBarre, M. J.; Raisimring, A.; Enemark, J. H. In *Molybdenum Enzymes, Cofactors and Model Systems*; Stiefel, E. I., Coucouvanis, D., Newton, W. E., Eds.; ACS Symposium Series 535; American Chemical Society: Washington, DC, 1993; pp 130–142.

(27) Basu, P.; Raitsimring, A. M.; LaBarre, M. J.; Dhawan, I. K.; Weibrecht, J. L.; Enemark, J. H. *J. Am. Chem. Soc.* **1994**, *116*, 7166–7176.

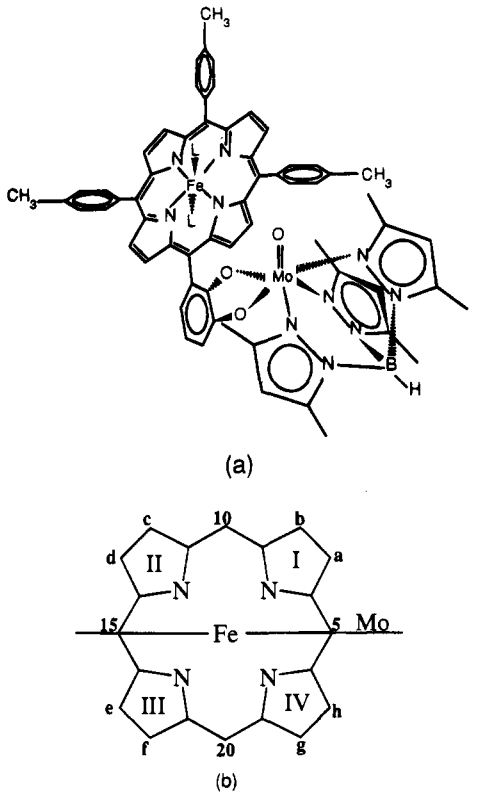

Figure 2. (a) Structure of the {tri-*p*-tolyl[2,3-[((hydrotris(3,5-dimethylpyrazolyl)borato)oxomolybdenum)dioxy]phenyl]porphyrinato}-bis(L)iron(III) complex, bis[Fe(2,3-Mo-TTP)(N-MeIm)$_2$]Cl, where L = *N*-methylimidazole. (b) Porphyrinate labeling system used for the pyrrole protons, *meso* positions, and pyrrole rings. This same numbering system has been used throughout the text for all complexes of this series. Note that the Mo(V) center is slightly off the C_5, C_{15} *meso* axis, and thus $H_a \neq H_h$.

investigation of spin coupling mechanism at low temperatures (4.2−77 K)[27,28] have previously been reported, show 6−8 resolved pyrrole-H resonances that do *not* coalesce as the temperature is raised. As we will show herein, the bulky (hydrotris(3,5-dimethylpyrazolyl)borato)oxomolybdenum(V) substituent, shown schematically in Figure 2a, effectively blocks the rotation of one axial ligand over the entire temperature range of the solvent. The paramagnetic oxomolybdenum(V) center has relatively long electron spin relaxation times (10^{-8}−10^{-9} s)[29] and thus also acts as a sensitive relaxation agent that aids in the unambiguous assignment of the eight resonances, arising from the eight pyrrole protons H_a−H_h, Figure 2b, which in turn allows complete mapping of the porphyrin π orbital preferred for unpaired electron spin delocalization from low-spin Fe(III) and estimation of the energy difference, ΔE_π, between it and its nondegenerate partner, which has roughly the opposite spin density distribution pattern, as shown in Figure 1. The exchange rates of the *anti* axial ligand of several complexes have also been measured and the results provide new and provocative information about their structures and energetics.

Experimental Section

Materials. All solvents for syntheses were purchased either from Aldrich or from Fisher and were distilled prior to use. NMR solvents (99.5% deuterated) were purchased from either Aldrich or Cambridge Isotopes and were dried over 4 Å molecular sieves. All syntheses were performed following the procedures described previously.[26,27] NMR samples were prepared in septum fitted screw cap NMR tubes (Wilmad) and thoroughly degassed with argon.

Syntheses. All high-spin Fe(III) complexes were synthesized following published procedures.[26,27] Low-spin complexes were generated in solution by adding the respective axial ligand base to a dichloromethane solution of the high-spin complex.[27]

Measurements. One-dimensional NMR spectra were recorded on either a Varian Unity 300 or a Bruker AM 500 spectrometer. The Varian spectrometer is equipped with SunSparc Stations where the data processing was performed. The Bruker instrument is networked with an IRIS computer system where some of the data were processed using FELIX software. Prior to the variable-temperature studies, the temperatures were calibrated with a standard methanol sample (Wilmad). Variable-temperature and relaxation measurements were performed on the Unity 300, whereas all the 2D and NOE difference experiments were performed on the AM 500 spectrometer. All samples were frequency-locked to solvent deuterium and referenced to the residual solvent proton signal. Typically, the one-dimensional spectra were acquired by using a spectral width of about 30 kHz, 16−32 K data points, 90° pulse width (~7−8 μs), 256−512 transients, and 0.25 s relaxation delay. The data were typically processed with 2−5 Hz exponential apodization before Fourier transformation.

Ligand Exchange Rates. Rate constants for axial ligand exchange were measured from NMR line broadening of the coordinated axial ligand methyl resonances.[30,31] Typically a 2−5 equiv excess of axial ligand was present in the solution. The *N*-methyl signals were observed in the range of 15−35 ppm depending on the temperature. The line widths were determined at half height using a line-fitting routine provided by Varian software (VNMR Version 4.1). The line widths of the pyrrole protons were also determined as a function of temperature. Since NMR data were obtained only in the slow exchange region, the preexchange lifetime, τ_i, in the site corresponding to the signal being observed, is given by La Mar[31,32] and others[33] as

$$\pi\Delta_{i,obs} = T'_{2i}{}^{-1} = T_{2i}{}^{-1} + \tau_i{}^{-1} \quad (1)$$

where $\Delta_{i,obs}$ is the line width at half height, $T'_{2i}{}^{-1}$ is the effective spin−spin relaxation time, and $T_{2i}{}^{-1}$ is the spin−spin relaxation time in the absence of exchange. The activation parameters were obtained by conventional Eyring plot methods.[34]

Relaxation Time Measurements. Solid samples were placed in Teflon-fitted screw cap NMR tubes (Wilmad) and purged with argon. Degassed dry solvent (CD_2Cl_2) was added under argon by means of a gas-tight syringe. Longitudinal relaxation times, T_1, were measured by the standard inversion recovery method with a RD−π−t_1−$\pi/2$− acquisition pulse sequence.[35] Typically, 128−256 transients were recorded with a 0.25 s relaxation delay (RD) corresponding to 15−20 times the longest T_1 of the pyrrole protons. The data acquired in this manner were processed and analyzed on the basis of standard exponential decay with the help of the Varian VNMR 4.1 software. The apparent transverse relaxation times (T_2*) were computed from the line widths at half height, or the true T_2 values were measured directly using the Hahn spin−echo pulse sequence. Relaxation times were measured at various temperatures; data at several temperatures are listed in Table S1, supporting information.

NOE Difference Measurements. Steady-state NOE measurements were performed on the Bruker AM 500 spectrometer using 50 mW

(28) Raitsimring, A. M.; Basu, P.; Shokhirev, N. V.; Enemark, J. H. *Appl. Magn. Reson.* Accepted for publication.
(29) Küsthart, U.; LaBarre, M. J.; Enemark, J. H. *Inorg. Chem.* **1990**, *29*, 3182−3187.
(30) LaMar, G. N.; Walker, F. A. *J. Am. Chem. Soc.* **1972**, *94*, 8607−8608.
(31) Satterlee, J. D.; La Mar, G. N.; Bold, T. J. *J. Am. Chem. Soc.* **1977**, *99*, 1088−1093.
(32) La Mar, G. N.; Sherman, E. O. *J. Am. Chem. Soc.* **1970**, *92*, 2691.
(33) (a) Emsley, J. W.; Feeney, J.; Sutcliffe, L. H. *High Resolution Nuclear Magnetic Resonance Spectroscopy*; Pergamon Press: London, 1965; Vol. 1, Chapter 9. (b) Binsch, G. In *Dynamic Nuclear Magnetic Resonance Spectrocopy*; Jackman, L. M., Cotton, F. A., Eds.; Academic Press: New York, 1975; Chapter 3.
(34) Wilkins, R. In *The Study of Kinetics and Mechanism of Reactions of Transition Metal Complexes*; Allyn and Bacon Inc.: Boston, 1974.
(35) (a) Levitt, M. H. *J. Magn. Reson.* **1982**, *48*, 234−264. (b) Derome, A. E. In *Modern NMR Techniques in Chemistry: Organic Chemistry Series*; Baldwin, J. E., Ed.; Pergamon Press: New York, 1987; Vol. 6, p 88.

irradiation power with a presaturation delay of 0.25 s. The spectra were recorded with a 50 kHz spectral bandwidth, 90° pulse width (7.3 μs) with 10 interleaved loops of on- and off-resonance irradiation, each having 128 transients. The off-resonance irradiation frequency was 11187 Hz greater than the highest observed frequency resonance (i.e., the methyl resonance of coordinated NMeIm). The differences of the time domain data were taken, followed by Fourier transformation with 5 Hz exponential apodization.

^{1}H COSY Spectra. Magnitude COSY[36,37] spectra were recorded on the Bruker AM 500 spectrometer at 30 °C using a spectral bandwidth of 17857 Hz, a mixing pulse of 90°, 256 t_1 increments, and 2K real data points, with 128 transients per t_1 data increment. Under these conditions the acquisition time was 57 ms. The spectral width of 17 857 Hz was chosen to cover only the pyrrole proton region; increasing the spectral width decreased the spectral resolution. With the small spectral width of 17 857 Hz, some of the resonances were folded, but the folded peaks did not overlap with the pyrrole resonances of interest. Prior to Fourier transformation, the 2D matrix in each dimension was multiplied by an unshifted sine-bell-squared window function and zero filled in t_1 to give a 2K × 2K matrix.

Results and Discussion

The porphyrin resonances of [Fe(2,3-Mo-TTP)L_2]$^+$Cl$^-$, where L = NMeIm, ImH, 4DAP, and of [Fe(3,4-Mo-TTP)(NMeIm)$_2$]$^+$Cl$^-$ have been studied by proton NMR spectroscopy over a wide temperature range. Of particular interest are the resonances of the pyrrole protons, which are known to reflect of the pattern of unpaired electron spin delocalization in paramagnetic metalloporphyrins.[1,10] We have mentioned earlier[27] that the molybdenum containing free base porphyrins show pyrrole proton resonances in the diamagnetic region (δ 8.83−8.95, multiplet) and that the chemical shifts are thus not significantly perturbed by the pendant paramagnetic molybdenum center. However, the resonances of the pyrrole protons closest to the Mo(V) center are severely broadened. The protons of the tris(3,5-dimethylpyrazolyl)borate ligand itself are too broad to be meaningfully interpreted. For complexes of the type [H_2(2,3-Mo-TTP)] and [Zn(2,3-Mo-TTP)] the pyrrole proton chemical shifts are extremely similar (δ 8.94, multiplet, Figure S1, supporting information), indicating negligible chemical shift modulation by the Mo(V) center. In contrast to the free base and Zn complexes, however, complexes of the type [Fe(2,3-Mo-TTP)L_2]$^+$Cl$^-$ (where L = NMeIm, ImH, 4DAP) and [Fe(3,4-MoTTP)(NMeIm)$_2$]$^+$Cl$^-$ show distinctive pyrrole proton resonances centered at −16.4 ppm at 23 °C, examples of which are shown in Figure 3.

For [Fe(3,4-MoTPP)(N-MeIm)$_2$]$^+$Cl$^-$, three clearly resolved pyrrole resonances and a very broad resonance are observed (Figure 3b); these four distinct resonances account for all eight pyrrole protons, and we observe only the effect of the unsymmetrical substitution pattern on the TTP ring.[10] This pattern has been observed previously for a number of monosubstituted [Fe(TPP)(NMeIm)$_2$]$^+$Cl$^-$ complexes.[3,10,18] However, for [Fe(2,3-MoTTP)L_2]$^+$Cl$^-$ (L = NMeIm), Figure 3a, seven clearly resolved resonances and an eighth very broad resonance (labeled 3) are observed for the eight pyrrole protons. Although the spread of the pyrrole-H resonances differs greatly for the 2,3- and 3,4-Mo-TTP isomers, the average shift of the resonances is identical (−16.4 ppm at 23 °C). This average pyrrole-H chemical shift compares well to those of other low-spin Fe(III) model hemes,[3] indicating that the chemical shifts are mainly affected by the low-spin Fe(III) center. Through-bond spin

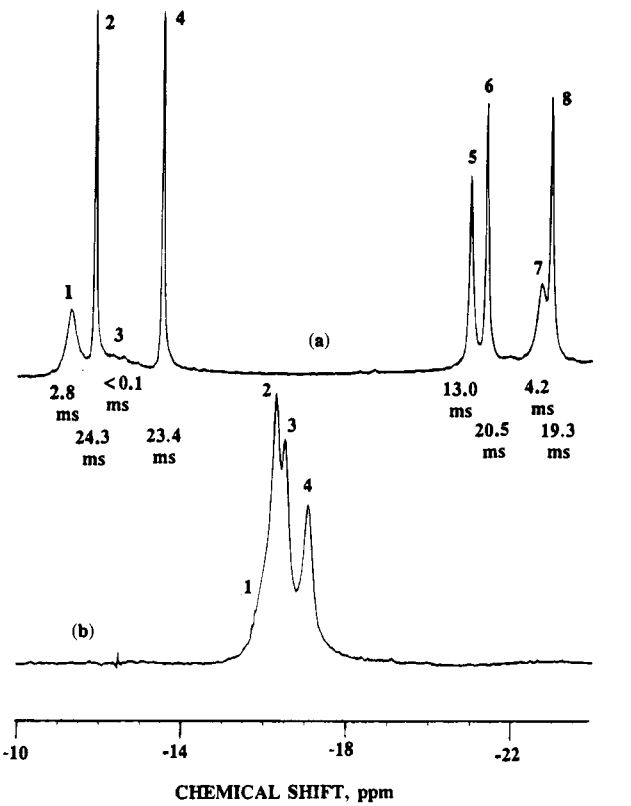

Figure 3. 500 MHz spectra of the pyrrole protons at 296 K in CD_2Cl_2 which clearly show the effect of the hindered axial ligand rotation. (a) [Fe(2,3-Mo-TTP)(NMeIm)$_2$]Cl, and (b) [Fe(3,4-Mo-TTP)(NMeIm)$_2$]-Cl with the peak numbering in increasing order from downfield to upfield. This is, not coincidentally, the order of increasing contact shifts of the pyrrole protons (see text).

delocalization from the Mo(V) center to the porphyrinate plane is prohibited by the symmetry of the d_{xy} orbital that contains the unpaired electron, as well as the orthogonality of the phenyl ring to which the Mo(V) center is bound, to the porphyrinate plane. The observation of a large number of pyrrole proton resonances for the [Fe(2,3-Mo-TTP)L_2]$^+$Cl$^-$ complexes raises the question of multiple structures for these complexes. We will show herein that the 1- and 2D NMR data clearly establish that all the observed pyrrole-H resonances arise from the same molecule and that the large number of pyrrole proton resonances are due to *a combination* of the very restricted rotation of the axial ligand *and* the inherent asymmetry of the porphyrinate ring that results from introduction of a very bulky asymmetric group at one *meso* position.

Pyrrole Proton Relaxation Time Measurements. Low-spin iron(III) porphyrinate complexes have one unpaired electron, which gives rise to strongly paramagnetically shifted proton NMR resonances, as discussed in many research publications and reviews.[1-10,37] The proton resonances observed are much broader than those of the corresponding diamagnetic analogues due to scalar and dipolar coupling with the unpaired electron spin. Electron spin relaxation times for low-spin Fe(III) are in the range of $10^{-11}-10^{-12}$ s,[38] and thus the resonances of ferriheme proteins and model complexes are usually well resolved, with large hyperfine shifts due to unpaired electron spin delocalization through the π system of the porphyrinate.[1]

The molecules investigated in the present study have one unpaired electron at the iron center and another unpaired electron

(36) Wemmer, D. E. *Concepts Magn. Reson.* **1989**, *1*, 59−72.

(37) (a) Yu, L. P.; La Mar, G. N.; Rajarathnam, K. *J. Am. Chem. Soc.* **1990**, *112*, 9527. (b) Keating, K. A.; deRopp, J. S.; La Mar, G. N.; Balch, A. L.; Shaiu, F.-Y.; Smith, K. M. *Inorg. Chem.* **1991**, *30*, 3258−3263.

(38) Bertini, I.; Luchinat, C. *NMR of Paramagnetic Molecules in Biological Systems*; Benjamin/Cummings: Menlo Park, CA, 1986; Chapter 3.

at the pendant molybdenyl center. Earlier studies demonstrated that at 77−4.2 K, the EPR spectrum of the low-spin Fe(III) center is strongly perturbed by the nearby unpaired electron of Mo(V) due to a weak exchange interaction ($J \sim 3-70 \times 10^{-3}$ cm^{-1}, 100−2000 MHz) between the unpaired electrons of the two paramagnetic centers.[27,28] However, under the conditions of the EPR measurements, the magnetic fields applied to the samples are much smaller (up to 4500 G or 0.45 T) than those used for NMR measurements (7.05−11.7 T). Thus, under the conditions used for NMR spectroscopy the electronic Zeeman interaction predominates over the exchange interaction, which is thus expected to be only a minor perturbation on the interaction between the unpaired electrons on low-spin Fe(III) and Mo(V). Observation of relatively sharp proton hyperfine shifted resonances supports the fact that magnetic interaction of the pendant Mo(V) center with the low-spin Fe(III) center is not a major contribution. It is therefore appropriate to treat the two paramagnetic centers separately, and thus, at the magnetic fields used for NMR spectroscopy, the paramagnetic pendant molybdenum(V) center acts as a dipolar relaxation agent for the pyrrole protons of the low-spin Fe(III) porphyrinate. The long electron spin relaxation times of oxoMo(V)[29] ensure that strongly distance-dependent ($\propto r^{-6}$) broadening of proton resonances will occur, as evidenced by the spectra shown in Figure 3. The stereochemical requirements of the molybdenyl center and its d_{xy}^1 electron configuration[39] both prohibit it from having direct through-bond spin delocalization with the porphyrin plane due to the bulky 3,5-dimethylpyrazolyl groups that restrict rotation about the $C_{meso}-C_{phenyl}$ bond for the 2,3-isomer, and the small spread of the pyrrole-H resonances of the free base (Figure S1, supporting information) and Zn(II) complexes confirms that the oxomolybdenum center does not produce contact shifts at the pyrrole-H positions.

We have measured the T_1 relaxation times of the pyrrole protons at different temperatures by inversion-recovery techniques (Figure S2, supporting information), and representative results are included in Figure 3a; T_2* relaxation times were calculated from the line widths of the resonances at half height or true T_2 values were measured directly using the Hahn spin−echo experiment. (In this system, because of the broad resonances and hence short T_2 relaxation times, $T_2^* \approx T_2$.) Relaxation time measurements were performed in order to achieve a complete assignment of the pyrrole-H resonances, which, as we will show, could not be achieved by 2D NMR techniques alone due to the short relaxation times of some of the resonances. The complete T_1 and T_2 relaxation data are presented in Table S1, supporting information.

From the relative line widths and T_1 values of the eight pyrrole-H resonances of [Fe(2,3-Mo-TTP)(NMeIm)$_2$]Cl summarized in Figure 3a and the data of Figure S2 and Table S1, it is apparent that peaks 2 and 4 have the longest T_1s whereas the T_1 of peak 3 is immeasurably short (<0.1 ms). Assuming that T_1s are dominated by dipolar relaxation and thus have a r^{-6} dependence of line width on distance from the relaxation agent(s),[40] peak 3 can be assigned to the proton closest to the Mo(V) center and peaks 2 and 4 to the protons farthest from the Mo center. From the relaxation data it is obvious that peaks 1 and 7 are also close to the Mo center, followed by peak 5 and then peaks 6 and 8. Since a crystal structure is not available for the complex, the distances of the pyrrole protons from the Mo atom were estimated using the molecular modeling program

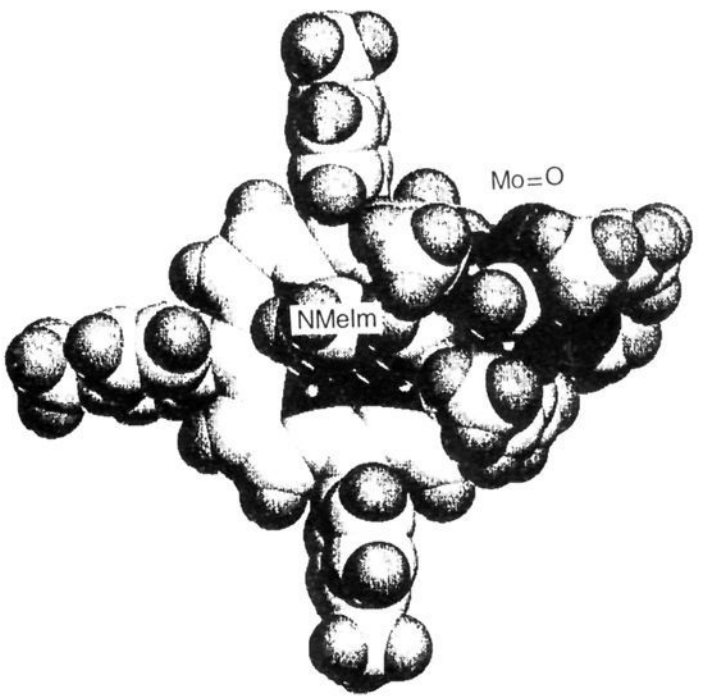

Figure 4. Space filling diagram of [Fe(2,3-Mo-TTP)(NMeIm)$_2$]$^+$ obtained from Sybyl energy minimization.[58]

Sybyl.[41] A space filling diagram of a minimized structure is shown in Figure 4. The Mo···pyrrole proton distances fall in the range 4.7−11.6 Å for [Fe(2,3-Mo-TTP)(NMeIm)$_2$]$^+$Cl$^-$, as summarized in Table 1.

To compare the distances obtained from molecular modeling (Table 1) to those estimated on the basis of the T_1 data presented in Figure 3a, Figure S2, and Table S1, we have attempted to correct the T_1s of the pyrrole protons caused by the unpaired electron of low-spin Fe(III) and the associated ligand-centered dipolar relaxation term due to spin delocalization to the β-pyrrole carbons.[40] La Mar and co-workers earlier published an apparent correlation between T_1 and the contact shifts of the heme methyl signals of 2,4-disubstituted deuterohemins.[40] They showed that, due to a ligand-centered dipolar contribution, $1/T_1$ follows a linear correlation with $(\delta_{con})^2$ (where δ_{con} is the contact contribution to the isotropic shift), having a slope of 0.03 s/ppm^2. Following the same methodology we have found a similar linear correlation between $1/T_1$ and the square of the contact shift of the directly bound pyrrole proton resonances in some unsymmetrically substituted low-spin Fe(III) tetraphenylporphyrinates,[10,42] with a slope of 0.02 s/ppm^2. The contact shift data for [Fe(2,3-Mo-TTP)L$_2$]Cl (see discussion below and Table 2) were then used to compute the relaxation times due to only the iron(III) center. These values were subtracted from the T_1 data of Table S1.

An empirical relation[43] was used to evaluate the total correlation time of the molecule, τ_c:

$$\tau_c^{-1} = \tau_r^{-1} + \tau_s^{-1} + \tau_m^{-1} \qquad (2)$$

(where τ_r is the rotational correlation time of the molecule, τ_s is the correlation time for electron spin relaxation, and τ_m is the exchange correlation time) in order to extract the contribution due to the Mo center from the T_1 data (Table 2). The value of τ_r was calculated from the Debye (Stokes−Einstein) expression,[43] which was used in eq 2 to extract the τ_c (assuming negligible chemical exchange processes and correlation due to spin relaxation). Experimental T_1/T_2 ratios were also used to

(39) Carducci, M. D.; Brown, C.; Solomon, E. I.; Enemark, J. H. *J. Am. Chem. Soc.* **1994**, *116*, 11856−11868.

(40) Unger, S. W.; Jue, T.; La Mar, G. N. *J. Magn. Reson.* **1985**, *61*, 448−456.

(41) Molecular modeling simulations were carried out on a Silicon Graphics IRIS system using the program SYBYL by Tripos Associates, Inc. The lowest energy van der Waals configurations were determined from the energy minimization routine MAXMIN2.

(42) Momot, K.; Walker, F. A. Unpublished data.

(43) Banci, L.; Bertini, I.; Luchinat, C. In *Nuclear and Electron Relaxation*; Weller, M. G., Maier, H. J., Eds.; VCH: Weinheim, 1991.

Table 1. Calculated[a] Pyrrole Proton Distances (in Å) from the Paramagnetic Mo(V) Center

complex	a	b	c	d	e	f	g	h
$[Fe(2,3\text{-Mo-TTP})(NMeIm)_2]^+$	4.74	6.35	10.11	11.33	11.57	10.64	7.42	5.58
$[Fe(2,3\text{-Mo-TTP})(ImH)_2]^+$	5.17	6.73	10.00	10.99	10.94	10.06	7.3	5.72
$[Fe(2,3\text{-Mo-TTP})(4DAP)_2]^+$	4.97	6.34	10.15	11.29	10.35	9.11	7.84	6.66
$[Fe(3,4\text{-Mo-TTP})(NMeIm)_2]^+$	5.82	8.30	13.14	14.52	14.64	13.36	8.72	6.20

[a] Obtained from energy minimization of the Sybyl molecular modeling program.[41]

Table 2. Calculated Distances (in Å) for Pyrrole Protons Obtained from T_1 Data

	peak no.[a]							
	1	2	3	4	5	6	7	8
$[Fe(2,3\text{-Mo-TTP})(NMeIm)_2]^+$	4.6	8.5	−b	8.5	7.4	8.1	4.4	8.0
proton position	h	d or e	a	e or d	g	c or f	b	f or c
ratio of distances (Sybyl/T_1)	1.2	1.3 or 1.4		1.4 or 1.3	1.0	1.25 or 1.31	1.4	1.33 or 1.26

[a] See Figure 3. [b] T_1 too short to measure (<0.1 ms).

obtain the correlation time (τ_c) from the Solomon equations.[44-46] All these methods indicate a correlation time in the range $5 \times 10^{-9} > \tau_c > 7 \times 10^{-10}$ s. We have used the latter value for estimating the proton distances from the Mo(V) center using the Solomon−Bloembergen (SB) equation.[47] The results are presented in Table 2, with the most likely assignments of the pyrrole protons based on T_1 data. The SB equation is used for estimation of the dipolar interaction because the 3-dimensional molecular stereochemistry does not allow much, if any, interaction of the Mo d_{xy} orbital with the porphyrin π system. (If the Mo center could delocalize its unpaired electron spin into the π system, the chemical shifts of the pyrrole protons close to Mo would be different, and the average pyrrole proton chemical shift would deviate significantly from that observed for the (3,4-Mo) complex and other low-spin TPPFe(III) complexes.[1]) The distances obtained from T_1 data (Table 2) are found to be slightly different (1−1.4 times) than those calculated from the molecular modeling (Table 1). Even though the distances are not reproduced quantitatively, the trends give us a qualitative idea of how the Mo center interacts with the pyrrole protons and aids in the pyrrole-H resonance assignment, as will be discussed further below.

COSY Experiments. Scalar connectivities between the pyrrole protons were established by two-dimensional ^1H COSY experiments performed for $[Fe(2,3\text{-Mo-TTP})(NMeIm)_2]^+\text{-}Cl^-$.[48-50] The COSY spectrum is displayed in Figure S3, supporting information. In principle, the eight pyrrole protons should give four sets of cross peaks due to the chemically inequivalent protons within each of the four pyrrole rings. Cross peaks are observed between resonances 2 and 6 and between 4 and 8, despite the relatively short relaxation times. Thus, these pairs of resonances are assigned to adjacent protons in two of the pyrrole rings. No COSY cross peaks were detected among resonances 1,3,5 and 7, due to their much shorter T_1 and T_2 relaxation times (Figure 3a; Figure S2 and Table S1, supporting information). Combining the relaxation and COSY data, one can conclude that resonances 4,8 and 2,6 are due to the pairs of two protons of the pyrrole rings that are farthest away from the Mo center, *i.e.*, rings II and III, Figure 2, while resonances 1,3,5 and 7 are due the protons of pyrrole rings that are closer to the Mo center, *i.e.*, rings I and IV.

1D NOE Difference Experiments. The chemically inequivalent protons of adjacent pyrrole rings should be coupled through space. Several attempts were made to detect NOEs by 2D NOESY and ROESY experiments at both 300 and 500 MHz, but under the experimental conditions employed it was not possible to detect cross peaks with significant intensity. The failure to observe clear NOEs in the 2D (NOESY and ROESY) experiments may be primarily due to the very short relaxation times of the pyrrole protons and the fact that these experiments measure transient NOEs or ROEs.[51] Therefore, we turned to steady-state 1D NOE difference experiments for the determination of through-space couplings. For steady-state experiments, the population difference is maintained during irradiation, and hence NOEs are more likely to be observed. Spin diffusion under conditions of steady-state irradiation should not be a major problem for these model compounds, due to the relatively small size (compared to proteins)[52] and thus their relatively short rotational relaxation times.

All 1D NOE difference experiments were performed at −30 °C or lower in order to ensure that ligand exchange is slow on the NMR time scale.[53] In these cases we do observe NOE enhancements between resonances 2 and 4. Representative spectra are shown in Figure 5. Note that the NOEs are negative, consistent with earlier results on less bulky derivatives of $[TPPFe(NMeIm)_2]^+$.[1,10] Another set of NOE enhancements also appear to be observed for resonances 5 (or 6) with 8 (or 7) (not shown), but peaks 5 and 6 are close enough to each other that one cannot rule out the possibility of partially irradiating both resonances; the same is true of 7 and 8. Therefore, we cannot say with certainty which resonance (5 or 6) is dipolar coupled to 8 and which to 7. However, observation of a clear NOE between resonances 2 and 4 further supports our initial assignment of the resonances on the basis of relaxation data, since it

(44) Solomon, I. *Phys. Rev.* **1955**, *99*, 559.

(45) Both Solomon (dipolar relaxation) and Solomon−Bloembergen (Curie relaxation) equations were employed to evaluate the correlation times assuming the entire relaxation is controlled by one or the other. However, neither extreme model is accurate. It has been mentioned[46] that in typical cases the influence of Curie spin on T_1 is quite small whereas it may be dominant in transverse relaxation.

(46) (a) Navon, G.; Valensin, G. In *Metal Ions in Biological Systems*; Sigel, H., Ed.; Marcel Dekker: New York, 1987; pp 1−45. (b) Gueron, M. *J. Magn. Reson.* **1975**, *19*, 58.

(47) (a) Bloembergen, N. *J. Chem. Phys.* **1957**, *27*, 575. (b) Solomon, I.; Bloembergen, N. *J. Chem. Phys.* **1956**, *25*, 261.

(48) Bertini *et al.*[49] recently questioned whether the COSY cross peaks in paramagnetic proteins are due to scalar coupling or Curie relaxation. Curie relaxation has been shown to be significant only for large paramagnetic proteins with very slow tumbling.[52] Hence, we are convinced that the cross peaks observed in the COSY map of Figure 4 are due to scalar coupling.

(49) (a) Bertini, I.; Luchinat, C.; Tarchi, D. *Chem. Phys. Lett.* **1993**, *203*, 445. (b) Bertini, I.; Luchinat, C.; Piccioli, M.; Tarchi, D. *Concepts Magn. Reson.* **1994**, *6*, 307−335.

(50) Qin, J.; Bax, A.; La Mar, G. N. *J. Magn. Reson.* **1993**, *102*, 332−336.

(51) Neuhaus, D.; Williamson, M. P. *The Nuclear Overhauser Effect in Structural and Conformational Analysis*; VCH Publishers Inc.: New York, 1989.

(52) Kumar, A., presented at the 5th Chianti Workshop on Magnetic Resonance, San Miniato, June 1993.

(53) Simonis, U.; Lin, Q.; Tan, H.; Barber, R. A.; Walker, F. A. *Magn. Reson. Chem.* **1993**, *31*, S133-S144.

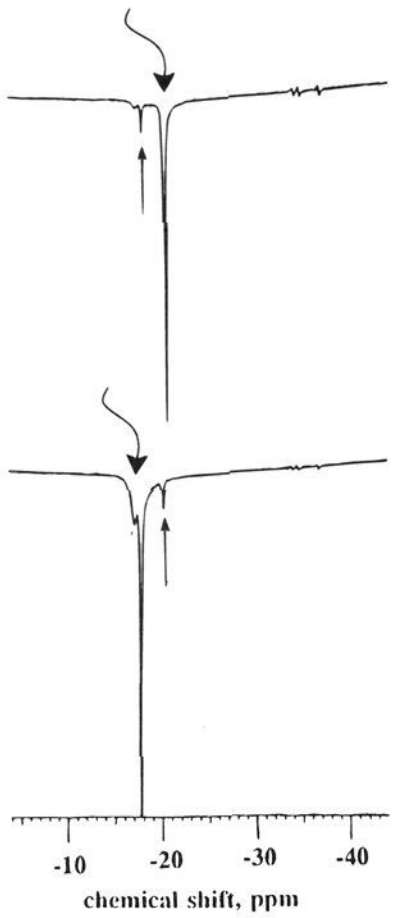

Figure 5. 500 MHz NOE difference spectra for [Fe(2,3-Mo-TTP)-(NMeIm)$_2$]Cl in CD_2Cl_2 at 215 K, showing the peak irradiated and the NOE observed. Only the experiments involving peaks 2 and 4 are shown.

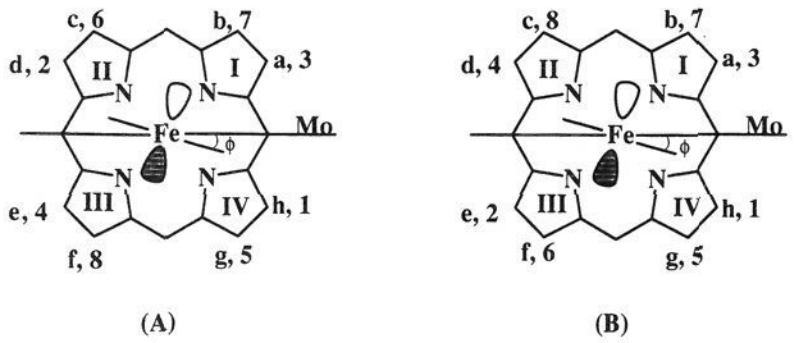

Figure 6. Two possible assignments of the pyrrole proton resonances. Part A shows the assignment most consistent with the isotropic shifts of the protons H_c, H_d, H_e, and H_f, as discussed in the text.

places protons 2 and 4 adjacent to each other in pyrrole rings II and III. Thus, at this point, we know that in pyrrole rings II and III, the order of protons must be 6,2,4,8 or 8,4,2,6, as shown in Figure 6, parts A and B, respectively.

Since the majority of the pyrrole resonances observed are correlated either by scalar coupling or by dipolar coupling, it can be concluded that the observed pyrrole resonances must arise from a single molecular species and not from multiple species with different structures.

Deduction of the Pattern of Contact Shifts from the NMR Spectra of the Pyrrole Protons. We have already mentioned that [Fe(2,3-Mo-TTP)(NMeIm)$_2$]$^+$Cl$^-$ shows eight distinct pyrrole-H peaks at 500 MHz (Figure 3a). The observed chemical shift of each proton (δ_{obs}) is composed of two parts as described in eq 3:

$$\delta_{obs} = \delta_{iso} + \delta_{dia} = \delta_{con} + \delta_{dip} + \delta_{dia} \quad (3)$$

The paramagnetic contribution to the observed shift is often called the isotropic or hyperfine shift and is referred to as δ_{iso} in eq 3. The diamagnetic shifts, δ_{dia}, of the pyrrole protons have been estimated from those of the free-base and Zn(II) complexes (Table 3) and span a range of no more than 0.2 ppm. The isotropic shift can be further split into two contributions, the contact (δ_{con}) and dipolar (δ_{dip}) shifts, as is also shown in

Table 3. Observed, Isotropic, Axial Dipolar, and Approximate Contact Shifts of [Fe(2,3-Mo-TTP)L$_2$]$^+$Cl$^-$ at 243 K in CD_2Cl_2

ligand	resonance	obsd shift (ppm)	isotropic shift (ppm)	axial dipolar shift (ppm)	approximate contact shift[a] (ppm)
NMeIm	1	−14.8	−23.7	−7.6	−16.1
	2	−15.5	−24.4	−7.6	−16.8
	3	∼−16.7	∼−25.8	−7.6	∼−18.0
	4	−17.6	−26.5	−7.6	−18.9
	5	−28.7	−37.6	−7.6	−30.0
	6	−29.2	−38.1	−7.6	−30.5
	7	−30.8	−39.7	−7.6	−32.1
	8	−31.1	−40.0	−7.6	−32.5
ImH	1,2	−20.5	−29.4	−7.4	−22.1
	3,4	−21.0	−29.9	−7.4	−22.5
	5	−24.0	−32.9	−7.4	−25.5
	6	−24.5	−33.4	−7.4	−26.0
	7,8	−25.5	−34.4	−7.4	−27.0
4DAP	1−3	−17.0	−25.9	−6.5	−19.4
	4	−17.8	−26.7	−6.5	−20.2
	5	−27.2	−36.1	−6.5	−29.7
	6	−27.7	−36.6	−6.5	−30.1
	7,8	−28.0	−36.9	−6.5	−30.4

[a] Calculated assuming that the rhombic dipolar shift is zero.

eq 3. Both contact and dipolar terms are expected to have inverse temperature dependence (for simple $S = 1/2$ systems in which only one orbital is thermally populated). The dipolar shifts are further subdivided into the axial and rhombic contributions:[54]

$$\delta_{dip} = (1/3)\{\chi_{zz} - (1/2)(\chi_{xx} + \chi_{yy})(3\cos^2\Theta - 1) + (3/2)(\chi_{xx} - \chi_{yy})(\sin^2\Theta)(\cos 2\Omega)\}r^{-3} \quad (4)$$

where r, Θ, and Ω are the polar coordinates that relate the position of the proton to that of the metal nucleus, and χ_{ii} are the principal values of the magnetic susceptibility tensor, in molecular units. The axial dipolar shift (first term in eq 4) can be evaluated using the methodology described previously.[1,55] Briefly, this methodology relies upon the fact that the 3e(π) orbitals of the porphyrin should have nodes at the *meso* carbons,[11] and therefore the phenyl-H resonance shifts are due almost entirely to the dipolar contribution.[1,55] Hence, using the *meta*-proton shifts and the geometric factors for the *m*-H and pyrrole-H positions (Table 1 of ref 1), the axial contribution to the dipolar shift can be calculated. In the present case, we have used the *meta*-H shift of [Fe(TPP)(NMeIm)$_2$]$^+$ because of the difficulty in assigning the multiple *m*-H shifts of [Fe(2,3-Mo-TTP)(NMeIm)$_2$]$^+$ and its diamagnetic Co(III) analog.

Calculation or estimation of the rhombic or in-plane contribution to the dipolar shift requires knowledge of the orientation of the in-plane magnetic axes of the complex, as will be discussed below. However, since the rhombic contribution to the dipolar shift is smaller than the axial contribution (*vide infra*), we can obtain the approximate contact shift of each of the pyrrole-H of the complexes of interest simply by subtracting the axial dipolar shift from the isotropic shift. The contact shifts of the pyrrole protons of [Fe(2,3-Mo-TTP)L$_2$]$^+$Cl$^-$ (L = NMeIm, ImH, 4DAP) at 243 K calculated according to this method are presented in the last column of Table 3. As is clear from the tabulated data, and as pointed out previously,[1] the contact term is by far the major contributor to the isotropic shift,[1]

(54) Jesson, J. P. In *NMR of Paramagnetic Molecules*; La Mar, G. N., Horrocks, W. D., Holm, R. H., Eds.; Academic Press: New York, 1973, pp 1−53.

(55) (a) La Mar, G. N.; Walker, F. A. *J. Am. Chem. Soc.* **1973**, *95*, 1782−1790. (b) La Mar, G. N.; Walker, F. A. In *The Porphyrins*; Dolphin, D., Ed.; Academic Press: New York, 1979; Vol. IV, pp 61−157.

and it is directly proportional to the unpaired electron spin density (ϱ_C) present in the p_π orbital of the carbon to which the proton is attached. The hyperfine coupling constants, A/h, in MHz, are related to the contact shifts of the protons of interest, δ_{con}, and the spin densities, ϱ_C,[54] by eq 5:

$$A_H/h = (T\delta_{con})[3\gamma_H k/2\pi g\beta S(S+1)] = Q\varrho_C/2S \quad (5)$$

where A_H is the Fermi contact coupling constant, γ_H is magnetogyric ratio of the proton, g is the electronic g-factor, β is the Bohr magneton, S is the effective spin, and $Q \sim -63$ MHz.[56] (We have used the simple McConnell equation value of Q (−63 MHz) because of the approximate nature of the calculations carried out in this study and the lack of evidence for negative spin density at the pyrrole-H positions of these low-spin Fe(III) porphyrinates.) Hence, the proton that gives rise to the largest contact shift (peak 8) is attached to the carbon that has the largest unpaired electron spin density. (We will postpone the actual calculation of spin densities until we have quantitatively accounted for the rhombic dipolar shift in a later section.)

Thus, peak 1 is due to the proton that has the smallest unpaired electron spin density, and spin density increases in the order 1 < 2 < 3 < 4 < 5 < 6 < 7 < 8. As is clear in Figure 3a, all eight peaks are observed in two groups: peaks 1−4 in one group have smaller spin densities and peaks 5−8 in the other group have much larger spin densities. Relaxation data permit assignment of peak 3 to proton "a" (H_a) in Figure 6, the proton that is closest to the MoO center. We further know from the 1D NOE difference spectra that resonances 2 and 4 are due to protons that are adjacent to each other and farthest away from the Mo center, *i.e.*, H_d and H_e in pyrrole rings II and III (or III and II, Figure 6, part A or B, respectively). Their scalar-coupled partner resonances 6 and 8 are due to the protons in the same pyrrole rings, and hence represent protons labeled H_c and H_f, respectively, in Figure 6, parts A and B. Since the resonances due to the protons of a given pyrrole ring appear in different groups, *i.e.*, the pattern of unpaired electron spin density within a given pyrrole ring is large−small, the three protons H_a, H_d, and H_e experience small unpaired electron spin density. Taken together, all of the evidence points to orbital b of Figure 1 as being the preferred π orbital for unpaired electron spin delocalization, and the ordering of the π orbitals is that shown on the left-hand side of Figure 1, as we have found previously for unsymmetrically *meso*-substituted TPP derivatives of low-spin Fe(III) having one relatively electron-withdrawing substituent.[10] Based upon this unpaired electron spin density distribution, the assignment of peaks 1 and 7, both of which have short and similar T_1 relaxation times, can be supported. Since resonance 1 has the smaller contact shift, it must be due to H_h, while resonance 7 is due to H_b. By process of elimination, resonance 5 must be due to H_g. The inability to observe an NOE with certainty for resonance 5 with 6 or 8 prohibits us from distinguishing pyrrole rings II and III, and thus two assignments of the eight pyrrole-H resonances are possible, as shown in Figure 6, parts A and B. We will discuss below that theoretical considerations favor the assignments shown in Figure 6A. However, in either case, the information we have presented thus far is enough to allow us to unequivocally assign the π orbital preferred for unpaired electron spin delocalization as belonging to the type shown in Figure 1, orbital b.

Careful inspection of the approximate contact shifts of the pyrrole protons of [Fe(2,3-Mo-TTP)(NMeIm)$_2$]Cl listed in the last column of Table 3 indicates that protons expected to have the same contact shifts in the absence of a fixed planar axial ligand (for example, H_a,H_h, resonances 3,1; H_d,H_e, resonances 2,4 or 4,2; H_b,H_g, resonances 7,5; H_c,H_f, resonances 8,6 or 6,8) actually appear to have contact shifts that differ by about 2 ppm. The trends are a > h, b > g, and we cannot yet define the trends for the protons in rings II and III. As will be shown below, these trends are indicative of the effects of the axial ligand plane and the asymmetric position of the molybdenyl center in defining the contact and rhombic dipolar contributions to the isotropic shift. First, however, we will consider the temperature dependence of the pyrrole-H shifts.

Temperature Dependence of the NMR Spectra. 1D ^{1}H NMR spectra of the complexes of type [Fe(2,3-Mo-TTP)L$_2$]Cl (where L = NMeIm, ImH, 4DAP), [Fe(2,3-OMe-TTP)(NMeIm)$_2$]-Cl, and [Fe(3,4-Mo-TTP)(NMeIm)$_2$]Cl in CD_2Cl_2 were obtained over most of the liquid range of the solvent (−90 to +30 °C). Representative spectra of [Fe(2,3-Mo-TTP)L$_2$]Cl at two different temperatures are displayed in Figure 7, together with their temperature dependence. As can be seen, over the entire temperature range of the present study the pyrrole proton resonances of [Fe(2,3-MoTTP)(NMeIm)$_2$]Cl do not cross each other or undergo coalescence. For [Fe(2,3-Mo-TTP)L$_2$]Cl (L = 4DAP and ImH), accidental overlap and crossover of some pyrrole-H resonances was observed, but again, no coalescence. This behavior contrasts with that of model hemes with one bulky *o*-phenyl substituent investigated previously, which exhibited coalescence of resonances indicating chemical exchange processes.[3] For [Fe(2,3-Mo-TTP)L$_2$]Cl, no chemical exchange process occurs, and thus at least one axial ligand is prevented from rotation over the entire temperature range studied. We also note that the [Fe(2,3-MoTTP)(NMeIm)$_2$]$^+$ complex shows the largest spread of the pyrrole proton resonances (11.24 ppm at 30 °C) followed by L = 4DAP (7.69 ppm at 30 °C) and L = ImH (5.62 ppm at 30 °C). In the case of [Fe(3,4-Mo-TTP)-(NMeIm)$_2$]Cl, quite a different situation exists: Four distinct pyrrole resonances are observed (Figure 3a), but unlike the 2,3-isomer, the spread of the pyrrole resonances is very small (0.91 ppm at 30 °C). This argues strongly that the large spread of the pyrrole proton resonances found for the complexes [Fe(2,3-Mo-TTP)L$_2$]Cl, as well as the observation of more than four pyrrole-H resonances in each case, is a result of hindered rotation of at least one of the planar axial ligands, NMeIm, ImH, or 4DAP.

It could be argued that another possible reason for observation of more than four pyrrole-H resonances might be the asymmetry of the axial NMeIm ligand. This possibility can be eliminated because the complex with the symmetrical axial ligand 4DAP (Figure 7c) exhibits 5−7 separate resonances, depending on temperature, leaving only the possibility that the steric bulk of the (tris(3,5-dimethylpyrazolyl)borato)oxomolybdenum group bound to the 2,3-positions of one phenyl ring of the tetraarylporphyrinate restricts the rotation of at least one axial ligand in [Fe(2,3-Mo-TTP)L$_2$]Cl.

In regard to the role of the electronic effect of the dioxyphenylmolybdenyl substituent, we have reported previously that both the equilibrium constants for NMeIm binding and the iron(III)/(II) reduction potentials of the 2,3- and 3,4- isomers are similar,[27] which suggests that the average electronic effect for the substituents of the two isomers is similar (or that a fixed axial ligand compensates for the difference in electronic effect), and thus the effect of unsymmetrical substitution on the spread of the resonances of the 2,3-isomer should not be significantly different from that observed for the 3,4-isomer. In the cases of both the 2,3- and 3,4-Mo substituents, however, both binding

(56) McConnell, H. M. *J. Chem. Phys.* **1956**, *24*, 764.

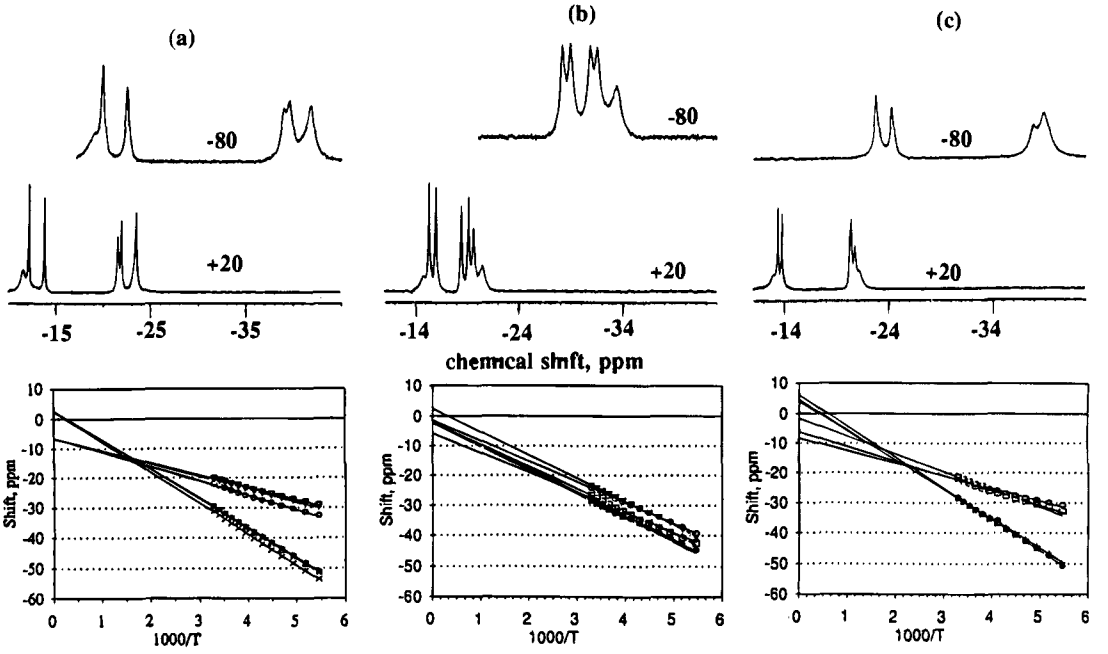

Figure 7. Representative spectra for the three $[Fe(2,3\text{-Mo-TTP})(L)_2]^+$ complexes (L = (a) NMeIm, (b) ImH, and (c) 4DAP) at two temperatures and the temperature dependences of the isotropic shifts measured at 300 MHz in CD_2Cl_2.

constants and reduction potentials suggest that the Mo substituent is slightly electron-withdrawing *with respect to the p-methyl substituents of the other three phenyl rings*, but that the difference in electronic effect is very small, and hence not the reason for the large spread of the pyrrole-H resonances for the complexes of interest (Figure 7). Thus, the effect of the substituents is expected to create relative energies of the two $3(\pi)$ orbitals a and b that are involved in unpaired electron spin delocalization as shown on the left side of Figure 1.

Thus, it is clear that the hindered rotation of one axial ligand of the 2,3-isomer plays a major role in determining the spread of its pyrrole proton resonances. In contrast, the relatively small spread of the pyrrole protons in $[Fe(3,4\text{-Mo-TTP})(NMeIm)_2]Cl$ suggests a low barrier to axial ligand rotation in this complex. If both axial ligands can rotate freely, and for the moment let us assume synchronously in parallel planes, then the interaction between the nitrogen π-donor orbital of each of the ligands and the d_π orbital of the metal that contains the unpaired electron will change as the ligands rotate. Alternatively, if the d_π orbital containing the unpaired electron remains aligned with the π orbital of the axial ligand nitrogens, then the d_π orbitals of the metal will rotate in concert with the axial ligands. If ligand rotation is fast on the NMR time scale of the possible differences in spin density produced by a particular alignment of the ligand plane, the effect of the planar ligands will be averaged and only the effect of unsymmetrical substitution of the porphyrinate ring will be observed. We believe this process describes the pyrrole resonance pattern for the 3,4-Mo isomer (Figure 3b).

In comparison, for the 2,3-isomer, $[Fe(2,3\text{-Mo-TTP})L_2]Cl$, if the axial ligands are aligned over the C_5,C_{15} *meso* carbons (where C_5 is the one that bears the unique substituent), then the node of the $3e(\pi)$ orbital that passes through those carbons will be aligned with the node of the nitrogen π orbitals of the two axial ligands. This axial ligand orientation will reinforce the situation created by the substituent effect, *i.e.*, small spin density at the carbons labeled a and h (as well as d and e) and large spin density at positions b, c, f, and g (left side of Figure 1, orbital b), and thereby maximize the spread of the pyrrole resonances. Alignment of the axial ligands over the *meso* positions at right angles to that of the unique substituent would enforce the choice of the other $3e(\pi)$ orbital (left side of Figure 1, orbital a). This orientation counteracts the substituent effect and will decrease the difference in spin delocalization, thereby leading to a smaller spread of the pyrrole proton resonances. It is clear, both from molecular modeling and from the T_1 data presented in Figure S2 and Table S1, that the axial ligands are approximately aligned with the node of the $3e(\pi)$ orbital that passes through the unique *meso* carbon (orbital b in Figure 1), and hence reinforce the difference in spin density distribution brought about by the unique substituent. In the case of $[Fe(2,3\text{-Mo-TTP})(NMeIm)_2]Cl$, the very large spread of the pyrrole peaks suggests a high rotational barrier for the axial ligands. The smaller spread of the pyrrole resonances for the corresponding 4DAP and ImH complexes suggests that in these cases, either there may be a somewhat lower barrier to rotation or, more likely, the lowest-energy orientation of the axial ligands differs from that of the NMeIm complex (or that the rhombic dipolar contribution is smaller (*vide infra*)).

In the previous two paragraphs we have assumed that for the 3,4-isomer the two axial ligands were in parallel planes and rotating synchronously. However, for the 2,3-isomer where the *syn* (adjacent) axial ligand is prevented from rotating, it could be that the *anti* (distant) ligand rotates rapidly, or that the two are held in perpendicular planes. The latter situation is possible in the case of the 4DAP complex[13] (and would certainly be the case for a bis(2-MeImH) or 1,2-Me_2Im complex[17]), while, for unhindered imidazoles such as NMeIm and ImH, the barrier to rotation is undoubtedly so low[13] that it is unlikely that the rotation is constrained to being synchronous. Thus, we conclude that, at least for the nonhindered imidazoles, although one axial ligand, the *syn* ligand, is strongly hindered from rotating, the other may be rotating very rapidly. Rapid rotation would average the effect of this *anti* ligand, and hence only the *syn* ligand would determine the spread of the pyrrole resonances. It is impossible to determine, from the data presented herein, whether the spread of the pyrrole resonances is determined by fixed orientation of only the *syn* ligand or both ligands in parallel planes. It should also be noted that the steric effect of the anion of this tight ion pair on axial ligand orientation may not be the same for all the complexes, and most notably for the ImH

Table 4. Isotropic, Axial, and Rhombic Dipolar, Corrected Contact Shifts and Spin Densities of $[Fe(2,3\text{-Mo-TTP})(NMeIm)_2]^+Cl^-$ at 243K in CD_2Cl_2

resonance	approx contact shift[a] (ppm)	$\phi = 0°$ [b] rhombic dipolar shift (ppm)	corrected contact shift (ppm)	assignment Figure 6A,B ($\phi = 0°$)	spin density from contact shift[c]	$\phi = +4°$ [d] rhombic dipolar shift (ppm)	corrected contact shift (ppm)	spin density from contact shift[e]	spin density from simple Hückel MO calcn[f]
1	−16.1	+3.6	−19.7	h, h	0.0095	+4.4	−20.5	0.0099	0.0053
2	−16.8	+3.6	−20.4	d, e	0.0101	+4.4	−21.2	0.0105	0.0058
3	∼−18.0	+3.6	∼−21.6	a, a	0.0105	+2.7	∼−20.7	0.0101	0.0058
4	−18.9	+3.6	−22.5	e, d	0.0110	+2.7	−21.6	0.0106	0.0062
5	−30.0	−3.6	−26.4	g, g	0.0130	−2.7	−27.3	0.0134	0.0124
6	−30.5	−3.6	−26.9	c, f	0.0132	−2.7	−27.8	0.0136	0.0126
7	−32.1	−3.6	−28.5	b, b	0.0140	−4.4	−27.7	0.0136	0.0125
8	−32.5	−3.6	−28.9	f, c	0.0142	−4.4	−28.1	0.0138	0.0131

[a] Calculated assuming that the rhombic dipolar shift is zero. [b] Calculated from eq 3 assuming that the principal magnetic axis in the plane is coincident with the C_5, C_{15} node. [c] Calculated from eq 4 using corrected contact shifts from column 4. [d] Calculated from eq 3 assuming clockwise rotation of the axial ligand by 4°. [e] Calculated from eq 4 using corrected contact shifts from column 8. [f] Calculated from eq 8 using orbital coefficients obtained from simple Hückel MO calculations[10] that assume $\alpha_{C5} = -0.3\beta_{CC}$, $\alpha_{C4,6} = -0.03\beta_{CC}$ and $\phi = +5°$.

complex, where the location of the chloride ion may be strongly influenced by hydrogen-bonding to one of the coordinated imidazoles.[57]

Role of Axial Ligand Plane Orientation in Determining the Rhombic Dipolar and Contact Shifts; Extraction of Spin Densities. It was mentioned above that the pattern of contact shifts reported in the last column of Table 3 suggests a needed correction due to the rhombic dipolar shift, arising from the orientation of the axial ligand plane and thus the in-plane magnetic axes. Using the axial ligand to define the orientation of the in-plane magnetic axes, we are able to account quantitatively for the rhombic dipolar shift and to correct the contact shifts reported in the last column of Table 3 in order to accurately calculate spin densities. The rhombic dipolar shift is given by:

$$\delta_{\text{rhomb.dip}} = (3/2)(\chi_{xx} - \chi_{yy})(\sin^2\Theta)(\cos 2\Omega)r^{-3} \quad (6)$$

where χ_{xx} and χ_{yy} are the magnetic susceptibilities along the in-plane magnetic axes, in molecular units, Ω is the angle from the minor in-plane magnetic axis (along χ_{xx}) to the proton of interest, and $\sin^2\Theta \approx 1$ for the pyrrole protons, since they are expected to be almost in the xy plane, even if the porphyrinate ring is slightly ruffled. The three principal values of the magnetic susceptibility tensor are difficult to measure, and hence, g-values are commonly used,[1,55] since $\chi_{ii} = g_{ii}2\beta^2S'(S' + 1)/3kT$ if the assumption is made that the complex of interest has only one thermally populated spin multiplet with effective spin S'.[54] This leads to the commonly-used expression:

$$\delta_{\text{rhomb.dip}} = \frac{\beta^2S'(S'+1)}{6kT}(g_{xx}^2 - g_{yy}^2)(\sin^2\Theta)(\cos 2\Omega)r^{-3} \quad (7)$$

However, as has been shown previously,[58] g-values obtained from EPR spectra at very low temperatures are not a good measure of the magnetic susceptibilities at the temperatures of NMR measurements due to second-order Zeemann contributions and thermal population of excited electronic states. Nevertheless, they will be used in this case as an approximate measure of the in-plane magnetic anisotropy, with the understanding that the actual value of $g_{xx}^2 - g_{yy}^2$ may be larger or smaller (or even of opposite sign[1]) than that calculated from EPR data, and thus the magnitude of the rhombic dipolar term may need to be scaled to this (unknown) value. (Calculations of the axial and rhombic anisotropies from the dipolar shifts of cytochrome c protein side chain protons have shown that in this case both values are smaller (81−95% and 51−66%, respectively) at ambient temperatures than those indicated by g-values measured at 4.2 K).[59] The $(\sin^2\Theta)(\cos 2\Omega)r^{-3}$ term is often called the rhombic geometric factor. If the in-plane symmetry axis is determined by the orientation of the p_π donor orbital of the axial ligand, and if that p_π orbital is aligned such that its nodal plane passes through the *meso* carbons C_5,C_{15} ($\phi = 0$ in Figure 6), then the rhombic geometric factors for the protons H_a,H_h and H_d,H_e are $\sim -0.5r^{-3}$, while those of the protons H_b,H_g and H_c,H_f are $\sim +0.5r^{-3}$. Based upon the size of the axial dipolar shift (Table 3) and the value of $g_{zz}^2 - (1/2)(g_{xx}^2 + g_{yy}^2)$ and $g_{xx}^2 - g_{yy}^2$ for $[Fe(TPP)(NMeIm)_2]Cl$ (4.50 and −2.86, respectively),[21] the rhombic dipolar shifts of the two groups of protons are +3.6 and −3.6 ppm, respectively, as listed in column 3 of Table 4. Correction of the contact shift by these amounts leads to the corrected contact shifts listed in the fourth column of Table 4. The possible assignments of these eight pyrrole proton resonances shown in Figures 6A and 6B, which differ in pyrrole rings II and III, are listed in the fifth column of Table 3. We note that for the assignment of Figure 6A, the calculated contact shifts vary in the manner a < e, h < d, b < f, and g < c, suggesting that the 2,3-Mo substituent is electron-withdrawing in nature, in agreement with the conclusion reached above. We also note that for the assignment shown in Figure 6A, a > h, e > d, b > g, and f > c, suggesting that, in order to cancel out the effect of the in-plane magnetic anisotropy, the axis of the rhombic dipolar contribution should be rotated by an angle ϕ in a clockwise direction, away from H_a and H_e (thereby decreasing their rhombic dipolar shifts and increasing their contact shifts) and toward H_h and H_d. For the assignment shown in Figure 6B, a > h, b > g, but e < d and f < c, and there is no rotation of the axial ligand plane that will cancel out these differences. On this basis, we believe that the assignment of the protons of rings II and III shown in Figure 6A is justified.

Assuming that the correct assignment is that of Figure 6A, rotation of the in-plane minor magnetic axis (the nodal plane of the axial ligand) *clockwise* by only 4° ($\phi = +4°$) leads to rhombic dipolar shifts for H_a,H_e of +2.7 ppm; for H_h,H_d of +4.4 ppm; for H_c,H_g of −2.7 ppm, and for H_b,H_f of −4.4 ppm, and the corrected contact shifts (column 8, Table 4) show a ∼ h; d ∼ e; b ∼ g; c ∼ f; *i.e.*, the effect of the ligand plane is nullified. Rotation of the g_{xx} axis by only half this amount (+2°) would divide the ∼2 ppm difference in shift of pairs of protons H_a,H_h;

(57) (a) Walker, F. A.; Lo, M. W.; Ree, M. T. *J. Am. Chem. Soc.* **1976**, *98*, 5552−5560. (b) Walker, F. A.; Balke, V. L.; West, J. T. *Frontiers in Bioinorganic Chemistry*; Xavier, A. V., Ed.; VCH: Weinheim, 1985; pp 183−193.

(58) Horrocks, W. D.; Greenberg, E. S. *Biochim. Biophys. Acta* **1973**, *322*, 38−44; *Mol. Phys.* **1974**, *27*, 993−999.

(59) Feng, Y.; Roder, H.; Englander, S. W. *Biochemistry* **1990**, *29*, 3494−3504.

H_dH_e; H_b,H_g; and H_cH_f (Table 4, column 4) between the rhombic dipolar and contact terms and thus simultaneously satisfy the expectations of both the contact and dipolar contributions to the isotropic shifts of these protons. Thus, the true contact shifts of the protons are probably the average of those given in columns 4 and 8 of Table 4, and the spin densities the average of those in columns 6 and 9. We have also calculated the spin densities in the two valence e(π) molecular orbitals from simple Hückel molecular orbital theory, assuming $\alpha_{C5} = -0.3\beta_{CC}$, $\alpha_{C4,6} = -0.03\beta_{CC}$ (negative values as would be expected for an electron-withdrawing substituent[10]), and $\phi = +5°$, and eq 8, to be discussed below, with $\Delta E_\pi = 160$ cm^{-1}. The results are presented in the final column of Table 4. The spin densities calculated in this manner are 55−95% of those observed, but the trends are qualitatively the same. We feel that this is acceptable agreement, considering the crudeness of the molecular orbital calculations and the uncertainty concerning the exact magnitude of the axial and rhombic dipolar shifts.

The contact shifts of the pyrrole protons in columns 4 and 8 of Table 4 clearly reveal that the reason for observation of eight pyrrole-H resonances is the combination of contributions to the rhombic dipolar and contact interactions due to the fixed orientation of a planar axial ligand. Furthermore, it is evident that the contact term dominates the isotropic shifts of the protons of these low-spin Fe(III) porphyrinate complexes; it is 3−4 times the size of the axial dipolar term, depending on proton location with respect to the nodal plane of the fixed planar axial ligand, and 5−10 times the size of the rhombic dipolar term, as calculated from EPR g-values.[21] Thus, even if the in-plane magnetic anisotropy is different at NMR temperatures than expected on the basis of g-values measured at 4 or 77 K, it is unlikely that the rhombic dipolar term could become large enough to dominate the isotropic shifts of low-spin Fe(III) porphyrinates. *Thus, it is likely that the spread of the methyl resonances in ferricytochromes c, b_5, and c_3 and other low-spin ferriheme proteins is controlled mainly by the effect of the orientation of the nodal plane of the strongest π donor ligand on the contact shift, rather than the effect of the in-plane magnetic anisotropy created simultaneously by that planar ligand and manifested in the rhombic dipolar shift.* As we will show in the next section, the axial ligand plane *also* has a major effect on the energy separation, ΔE_π, between the two orbitals of Figure 1, and is thereby responsible for the very large spread of the pyrrole-H resonances, as illustrated in Figure 3a.

Curie Behavior. It has been shown previously that P→M π bonding (resulting in π electron delocalization from the porphyrin filled 3e(π) orbitals to the e-symmetry d_π orbitals) is dominant for low-spin Fe(III).[1,10,55] With unsymmetrical substitution at the *meso* position the two 3e(π) and d_π orbitals are no longer degenerate.[1,4] The hindered rotation of one axial ligand can also break the degeneracy.[1,4] The relative energy of the two resulting non-degenerate orbitals (outside portions of Figure 1) determines which orbital is preferred for spin delocalization, and the energy separation between them (ΔE_π) determines to what extent each orbital is populated at a given temperature.[4,7,10] As we have shown above, the temperature dependence of the pyrrole proton peaks of the complexes [Fe(2,3-Mo-TTP)(NMeIm)$_2$]Cl, [Fe(2,3-Mo-TTP)(ImH)$_2$]Cl, and [Fe(2,3-Mo-TTP)(4DAP)$_2$]Cl over the range −90 to +30 °C shows that although the isotropic shifts vary linearly with inverse temperature, the extrapolated intercepts are non-zero (Figure 7). Furthermore, as observed previously,[3,60] for the NMeIm and 4DAP complexes, the straight lines tend to cross at $1/T \sim 2 \times 10^{-3}$ K^{-1} or $T \sim 500$ K. Similar behavior has been observed previously for a number of other model hemes[3,60] and heme proteins.[7,61] These deviations from Curie behavior are known to be a result of thermal population of excited states,[55,58] which give rise to linear temperature dependence, but with non-zero intercepts.[60] However, the nature and number of these excited states has not previously been clearly defined.

As we have shown recently,[4] the temperature dependence of these model hemes and heme proteins can be reproduced quantitatively by considering only one excited state, which arises from excitation of one of the paired electrons of the "other" e(π) orbital of Figure 1 to the half-filled valence orbital. The energy separation between these two orbitals may be as little as several tens of cm^{-1},[1,4,10] or as much as ~200−800 cm^{-1}.[2,4,7] The "other" near-valence e(π) orbital has the opposite pattern of spin densities from that of the HOMO, as shown in Figures 1a and 1b. The populations of these two e(π) valence orbitals are thus governed by the Boltzmann distribution, and because of the expected relatively small difference in energy as compared to kT, both levels will contribute significantly at the temperatures of these NMR experiments. The expected temperature dependence of the minimum of four (or in the present case, up to eight) pyrrole-H resonances can be calculated from eq 8,[4] which assumes that the unpaired electron is distributed between two energy levels (1) and (2) corresponding to those shown on either the left- or right-hand outside portions of Figure 1 on the basis of the Boltzmann distribution, with the resulting shifts following the Curie law:

$$\delta_n^{con} = \frac{F}{T}\frac{W_1 C_{n1}^2 + W_2 C_{n2} 2e^{-\Delta E\pi/kT}}{W_1 + W_2 e^{-\Delta E\pi/kT}} \qquad (8)$$

where the C_{n1} and C_{n2} are the molecular orbital coefficients ($C_{n1}^2 = \varrho_{Cn1}$, for example) calculated for each β-pyrrole position (C_a−C_b) for each of the two levels 1 and 2; W_1 and W_2 are the statistical weights for each orbital; ΔE_π is the energy separation of the two levels; and F is $(-63\text{ MHz})\pi g\beta_e/2k\gamma_H = -4.968 \times 10^5$ ppm K. For the systems of interest herein, $W_1 = W_2$.[4] As was shown above, the best fit is obtained if we assume that the equilibrium position of the *syn* axial ligand is ~2° away from the C_5−C_{15} *meso* axis in the direction of C_b (clockwise rotation). The effect of this non-alignment of substituent and axial ligand nodal planes on the contact contribution to the isotropic shifts creates the eight different pyrrole-H spin densities observed as eight different contact shifts.

The most dramatic effect created by the fixed planar axial ligand in these systems is to increase the energy difference ΔE_π between the two 3e(π) orbitals to a much greater extent than is observed in the case of unsymmetrical substitution in the porphyrin plane in the presence of freely-rotating axial ligands.[1,4,10] The nodal plane of the valence e(π) orbital that contains the unpaired electron is aligned with the nodal plane of the axial ligand, slightly shifted from the *meso* C_5,C_{15} axis, as shown in Figure 6A. We had earlier predicted, on the basis of the g-values of low-spin Fe(III) porphyrinates with planar axial ligands,[2] that the maximum difference in energy of the two d_π orbitals (and hence the two valence e(π) orbitals) is about 2λ, where λ is the spin−orbit coupling constant for low-spin Fe(III). This value has been variously estimated as 200−400 cm^{-1},[2] leading to a maximum difference in energy of the two orbitals of ~800 cm^{-1}. The temperature dependence of the contact shifts of the pyrrole protons of [Fe(2,3-Mo)TTP(NMeIm)$_2$]$^+$ having one fixed axial ligand aligned as shown in

(60) Walker, F. A.; Benson, M. *J. Phys. Chem.* **1982**, *86*, 3495−3499.

(61) Peyton, D. H.; La Mar, G. N.; Pande, U.; Ascoli, F.; Smith, K. M.; Pandey, R. K.; Parish, D. W.; Bolognesi, M.; Brunori, M. *Biochemistry* **1989**, *28*, 4880−4887.

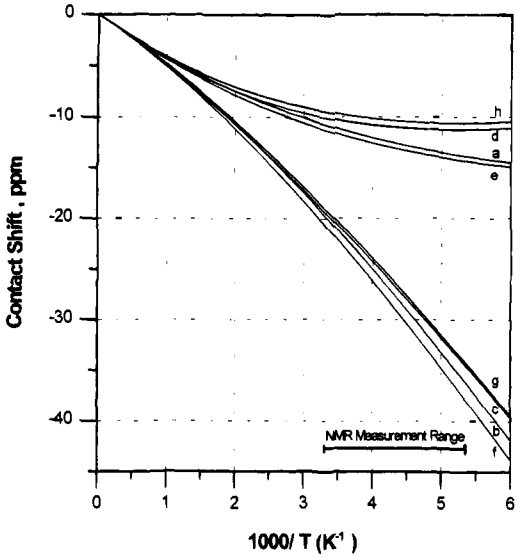

Figure 8. Plot of the calculated (eq 8) Curie behavior for an unsymmetrically *meso*-substituted iron(III) tetraphenylporphyrinate with a reasonably-chosen (but not necessarily quantitatively correct) set of orbital coefficients, a planar axial ligand fixed in orientation 5° clockwise from the C_5,C_{15} *meso* axis, and an energy separation of the two formerly-degenerate π-symmetry valence orbitals, $\Delta E_\pi = 160\ cm^{-1}$. This calculated temperature dependence may be compared to the linear Curie behavior assumed to be the case on the basis of the isotropic shifts measured over the temperature range +30 to - 90 °C for the complexes having *N*-MeIm or 4-DAP shown in Figure 7 (labeled "NMR measurement range" in this figure). If the data of this figure are assumed to follow linear Curie dependence over the NMR measurement range, they cross at $1000/T \approx 1.5-2.0$, as is observed experimentally for [Fe(2,3-Mo-TTP)(NMeIm)$_2$]$^+$Cl$^-$ and [Fe(2,3-Mo-TTP)(4DAP)$_2$]$^+$Cl$^-$ (Figure 7, parts a and c).

Figure 6 has been calculated using eq 8 with various energy separations, ΔE_π. Such a calculated temperature dependence is shown in Figure 8, where the approximate matching of pyrrole-H contact shifts was achieved by assuming that the energy difference is considerably smaller ($\sim$160 cm^{-1}) than the maximum. This likely indicates that the axial ligand is not held as rigidly in one exact position as we might have assumed on the basis of the Sybyl energy minimizations mentioned above and shown in Figure 4. Note, however, that although the thermal population of the two e(π) orbitals predicts that the temperature dependence will be curved, over the experimental range of the NMR measurements, the curvature is predicted to be small enough that one would be tempted to impose linear $1/T$ dependence on the data obtained. If this is done using the calculated lines of Figure 8, the apparent intercepts obtained are non-zero (lines not shown in Figure 8), as observed for the experimental data of Figure 7, and the lines cross at approximately $1/T = 2 \times 10^{-3}$ K^{-1}, as is also observed for the experimental data of Figure 7.

Comparison to a Protein. La Mar and co-workers have reported variable-temperature ^{1}H NMR of native *Aplysia* met-MbCN and reconstituted *Aplysia* met-MbCN.[61] The Curie plots of the methyl protons show intercepts either upfield or downfield of the diamagnetic shift expected for these resonances, and the lines cross each other at $1/T \sim 2 \times 10^{-3}$. The authors suggested that the reason for "non-Curie" intercepts could be "the dynamic averaging over one or more structures with somewhat different contact shift patterns".[61] In the present study we have clearly shown that with only one structure, having one thermally accessible excited state created by population of the "other" near-valence e(π) orbital, Figure 1, the pyrrole proton resonances can show "linear" temperature dependence based upon extrapolation of shifts obtained over the NMR-accessible temperature range, with intercepts positive or negative of their diamagnetic shifts and the individual lines cross at $1/T \sim 2 \times 10^{-3}$ in the straight line approximation of $1/T$ dependence. Equation 8 thus explains the apparent deviations from simple Curie behavior[61] without the assumption of multiple structures of the heme protein.

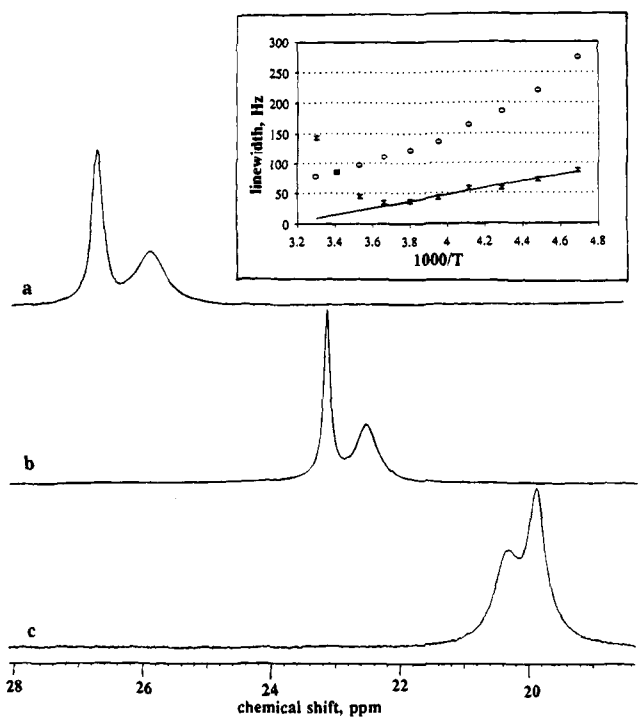

Figure 9. NMR traces of the methyl resonances of the coordinated axial ligands of [Fe(2,3-Mo-TTP)(4DAP)$_2$]$^+$Cl$^-$ at three representative temperatures recorded at 300 MHz in CD_2Cl_2: T = 243 (a), 273 (b), and 303 K (c). Inset: The temperature dependence of the line widths of the same resonances—(×) *anti* ligand; (○) *syn* ligand. The excess line width at each temperature is equal to the rate constant for ligand exchange.

Ligand Exchange Rates. The methyl signals of coordinated NMeIm and 4DAP were assigned by comparison to the reported chemical shifts of these ligands for other systems[30,31] and by comparing the relative integrated intensity (6 and 12, respectively) with that of the pyrrole protons (8). The two methyl signals of coordinated NMeIm have very different T_1s, as seen in the inversion recovery experiments (supporting Figure S2). At high temperatures, the more upfield-shifted methyl peak has a shorter T_1 which is broader than the downfield-shifted peak. Upon lowering the temperature, the relatively sharper downfield peak sharpens and then begins to broaden severely. (Plots of the chemical shifts of these protons *vs* $1/T$ demonstrate clearly that the proton resonances do not cross each other over the temperature range of the NMR spectral measurements.) This temperature dependance of the line width, together with the relative broadness of the two peaks at low temperatures where axial ligand exchange is slow on the NMR time scale, allowed us to assign the resonances unambiguously. The upfield peak is due to the ligand on the same side of the porphyrin as the Mo(V) center (*syn*), while the downfield peak is due to the ligand on the opposite side of the porphyrin plane (*anti*). In the case of [Fe(2,3-Mo-TTP)(4DAP)$_2$]Cl at 30 °C, the upfield signal is broader than the downfield one at high temperatures, as shown in Figure 9. The downfield signal narrows upon lowering the temperature and then again broadens. Again, there is no crossover of resonances. The upfield resonance showed monotonic broadening (Figure 9) with decreasing temperature,

Scheme 1

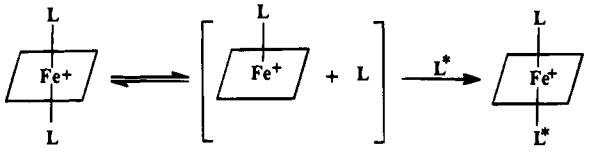

Scheme 2

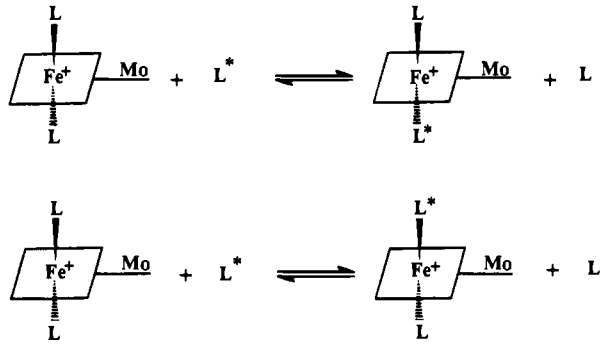

Table 5. First-Order Rate Constants for Axial Ligand Exchange (k_{ex} in s^{-1})

complex	temp, °C			
	30	20	10	0
$[Fe(2,3\text{-Mo-TTP})(4DAP)_2]^+Cl^-$	843	440	142	36
$[Fe(2,3\text{-Mo-TTP})(NMeIm)_2]^+Cl^-$	243	96	39	
$[Fe(3,4\text{-Mo-TTP})(NMeIm)_2]^+Cl^-$	269	105	43	14

thus allowing us to assign this signal as that arising from the ligand *syn* to the Mo(V) center. It is also worth mentioning that the methyl resonance of the *syn* ligand in [Fe(2,3-Mo-TTP)-(NMeIm)$_2$]Cl is broader than that of the corresponding ligand in [Fe(2,3-Mo-TTP)(4DAP)$_2$]Cl. This indicates that the methyl group of the *syn* NMeIm is closer to the Mo(V) center than the methyl groups of the *syn* 4DAP. The pertinent Mo···C-(methyl) distances obtained from molecular modeling are ~4.7 Å for NMeIm and ~5.6 and ~7.5 Å (average = 6.6 Å) for 4DAP.

From the differential broadening of the coordinated ligand methyl resonance with temperature it was possible to estimate the exchange rates of one axial ligand as a function of temperature. The methodology for this measurement of ligand exchange rates using NMR line broadening techniques in the slow exchange limit has been delineated elsewhere.[31] It was also shown that the axial ligand exchange process is a first-order dissociative process.[30,31] Thus the ligand exchange rate does not depend on the concentration of excess axial ligand. The probable ligand exchange process is shown in Scheme 1. In principle, for the unsymmetrical molecules of the present study, there exist two ligand exchange processes (Scheme 2). The rate of one of such process, namely the exchange rate of the ligand on the opposite (*anti*) side from the Mo(V) center (Figure 9), could be determined for [Fe(2,3-Mo-TTP)L$_2$]Cl (L = NMeIm, 4DAP). The monotonic behavior of the line width of the *syn* ligand's methyl group in each case did not allow us to measure the rate constant of that process (Table 5). This indicates that the *syn* ligand exchange rate is much slower than that of the *anti* ligand on the NMR time scale. It has previously been suggested that the *syn* axial ligand exchange rate is slower than that of the *anti* ligand in the case of *ortho*-substituted metalloporphyrins,[3,62] and for the first time, the Mo(V) relaxation probe allows us to demonstrate this unequivocally.

(62) Collman, J. P.; Brauman, J. I.; Fitzgerald, J. P.; Sarapany, J. W.; Ibers, J. A. *J. Am. Chem. Soc.* **1988**, *110*, 3486.

Table 6. Activation Parameters for Axial Ligand Exchange in CD_2Cl_2

	$\Delta H^{\ddagger}$ [a]	$\Delta S^{\ddagger}$ [a]	$k_{ex,298}$, s^{-1}
$[Fe(2,3\text{-Mo-TTP})(4DAP)_2]^+Cl^-$	19 (±2)	20 (±2)	802
$Fe(2,3\text{-Mo-TTP})(NMeIm)_2]^+Cl^-$	15 (±1)	3 (±2)	163
$[Fe(3,4\text{-Mo-TTP})(NMeIm)_2]^+Cl^-$	16 (±1)	5 (±2)	179
$[Fe(TPP)(NMeIm)_2]^+Cl^-$ [c,d]	20 (±2)	9 (±3)	66
$[Fe((o\text{-}OCH_2C_6H_5)_1TPP)(NMeIm)_2]^+Cl^-$ [d,e]	19 (±2)	14 (±2)	48
$[Fe((o\text{-}CONMe_2)_1TPP)(NMeIm)_2]^+Cl^-$ [d,e]	16 (±1)	3 (±2)	57
$[Fe((o\text{-}CON(C_6H_{12}))_1TPP)(NMeIm)_2]^+Cl^-$ [d,e]	16 (±2)	3 (±3)	67
$[Fe((o\text{-}CON(C_8H_{14})_1TPP)(NMeIm)_2]^+Cl^-$ [d,e]	15 (±1)	1 (±1)	60

[a] In kcal/mol. [b] In eu. [c] Data taken from ref 31. [d] Measured in $CDCl_3$. [e] Data taken from ref 3.

Assuming that the same pattern does indeed hold for the *ortho*-substituted $[Fe(TPP)(NMeIm)_2]^+$ complexes reported previously, the rate constants for exchange of the *syn* ligand in the best understood of those complexes range from 8 to 20 s^{-1} at 25 °C while the rate constants for the *anti* ligands range from 33 to 67 s^{-1}.[3]

The temperature dependence of the coordinated ligand resonance line widths of [Fe(3,4-Mo-TTP)(NMeIm)$_2$]Cl was also studied. In this case, however, only one single methyl peak from coordinated NMeIm was observed, with the integral corresponding to 6 protons, indicating that the unsymmetrical substituent is close enough to the plane of the porphyrinate ring that the *syn* and *anti* ligands are not different in chemical shift or line width. It should also be noted that we did not observe any significant difference in the rate constants between [Fe-(2,3-Mo-TTP)(NMeIm)$_2$]Cl and [Fe(3,4-Mo-TTP)(NMeIm)$_2$]Cl, which indicates that a possible doming effect, as discussed in ref 3, apparently does not play a key role in this type of complex. However, the *anti* ligand of each of the complexes shows larger rate constants for exchange than does [Fe(TTP)(NMeIm)$_2$]Cl[31,63] or other related complexes,[3] mainly as a result of smaller enthalpies of activation for ligand exchange in the present complexes than for symmetrical Fe(III) tetraphenylporphyrinates[31] and larger entropies of activation than other complexes having one bulky *ortho* substituent[3] (Table 6). Smaller enthalpies of activation indicate that the metal−ligand bond strengths of the *anti* ligands in the complexes of the present study are less than those of the symmetrical TTP complex studied previously,[31] but the bond strengths are similar to those of other mono-*ortho*-substituted TPP complexes.[3] Considering the inherent errors in measurement of activation parameters, the bond strengths of *anti* ligands in most unsymmetrically substituted Fe(III) TPPs appear to be similar, and smaller than those of *syn* ligands.[3]

We also notice that for [Fe(2,3-Mo-TTP)L$_2$]Cl (L = NMeIm, 4DAP) the rate constant for the exchange of the *anti* ligand of the 4DAP complex is almost 4 times larger than that of the NMeIm complex. La Mar and others have shown, with various bulky ligands, that the ligand exchange rate increases with an increase in the steric bulk of the ligand.[31] It is to be expected that as the steric crowding increases the compound tends to release the strain by releasing the ligand, making the complex more labile. The effect of a 6-membered as compared to a 5-membered heterocyclic ring is to increase the steric bulk in the bis(4DAP) complex as compared to that of the bis(NMeIm) complex.

Summary and Conclusions. Detailed NMR investigations of the novel compounds $[Fe(2,3\text{-Mo-TTP})L_2]^+Cl^-$ have been carried out. We have shown that a combination of unsymmetrical *meso* substitution and hindered axial ligand plane

(63) Note that the solvent used in ref 31 was $CDCl_3$ rather than CD_2Cl_2, as in the present study.

orientation can give rise to as many as eight distinct pyrrole-H resonances that arise from a single iron(III) porphyrinate species. Although the unpaired electron of the pendant oxomolybdenum center is involved in a weak exchange interaction with that of the low-spin Fe(III) center,[28] at the high magnetic field of the NMR experiments, Mo(V) acts primarily as an effective differential dipolar relaxation agent in these molecules. Such a relaxation agent greatly facilitates the assignment of pyrrole-H resonances. The pattern of contact shifts for the pyrrole protons allows us to estimate the unpaired electron spin density at each pyrrole carbon position. A combination of COSY, NOE difference spectroscopy, the T_1 and T_2 relaxation time measurements, and the spin densities delineate accurately the preferred orbital for spin delocalization to be (b) in Figure 1 and allows all pyrrole-H resonances to be assigned. Using arguments based upon the behavior of the (small) rhombic dipolar contribution to the isotropic shift, the final, unambiguous assignment of the pyrrole-H can be achieved (Figure 6A). The apparent deviation from Curie behavior (non-zero intercepts) can be explained by invoking a simple treatment of mixing two nondegenerate orbitals (eq 8). A planar ligand or other strong donor ligand having a p_π filled orbital enforces a much larger energy difference, ΔE_π, between the two nondegenerate valence orbitals than can be obtained simply from unsymmetrical substitution on the periphery of the porphyrinate ring, suggesting that such a two-orbital treatment is sufficient to explain the temperature dependence of the heme methyl resonances of *Aplysia* met-MbCN.[61] We have also shown the relatively small effect of the orientation of the nodal plane of the ligand on the in-plane (rhombic) magnetic anisotropy and its much larger effect on spin delocalization *via* the contact interaction. Thus, it is likely that the spread of the methyl resonances in ferricytochromes b_5 and *c* and other low-spin ferriheme proteins is controlled largely by the effect of the orientation of the nodal plane of the strongest π donor ligand on the *contact* shift, rather than on the in-plane magnetic anisotropy created simultaneously by that same planar ligand and manifested in the rhombic dipolar term.

The rate constant for axial ligand exchange was found to be largest for the *anti* ligand of $[Fe(2,3\text{-Mo-TTP})(4DAP)_2]^+Cl^-$, and the Mo(V) center was again extremely valuable as a relaxation agent in allowing assignment of the methyl resonances due to *syn* and *anti* axial ligands. Because of the relaxation properties of the Mo(V) center, it was possible to show unequivocally that the *anti* ligand exchanges much more rapidly than the *syn* ligand.

Acknowledgment. The authors acknowledge Dr. Arnold M. Raitsimring for helpful discussions regarding electron spin relaxation processes, Professor Mario Rivera for 2-D NMR experimental assistance, Mr. Konstantin Momot for providing his T_1 data for unsymmetrical $[Fe(TPP)(NMeIm)_2]^+$ complexes before publication, Professor Donald A. Tarr for developing the drawing for Figure 1, and Professor Ursula Simonis for many helpful comments. We also thank Professor W. Robert Scheidt for a preprint of ref 37 and Professor Marco A. Lopez for one of ref 43. Financial support of this work received from NIH grants GM-37773 (J.H.E.) and DK-31038 (F.A.W.) and NSF CHE-9214383 for purchase of the Unity-300 NMR spectrometer is gratefully acknowledged.

Supporting Information Available: Figure S1, ^1H NMR spectra of the free base porphyrins $[H_2(2,3\text{-Mo-TPP})]$ and $[H_2(3,4\text{-Mo-TTP})]$, Figure S2, example of inversion-recovery data utilized to measure the T_1 relaxation times of $[Fe(2,3\text{-Mo-TTP})(NMeIm)_2]^+Cl^-$, and Figure S3, COSY spectrum of the pyrrole-H region of $[Fe(2,3\text{-Mo-TTP})(NMeIm)_2]^+Cl^-$; Table S1, summary of T_1 and T_2 relaxation data obtained for the complexes of this study (5 pages). This material is contained in many libraries on microfiche, immediately follows this article in the microfilm version of the journal, and can be ordered from the ACS, and can be downloaded from the Internet; see any current masthead page for ordering information and Internet access instructions.

JA951045G